Chemical characterization and biological effect of exopolysaccharides synthesized by Antarctic yeasts Cystobasidium ongulense AL_{101} and Leucosporidium yakuticum AL_{102} on murine innate immune cells

Snezhana Rusinova-Videva (jrusinova@abv.bg)
Stephan Angeloff Institute of Microbiology
Manol Ognyanov
Institute of Organic Chemistry with Centre of Phytochemistry
Yordan Georgiev
Institute of Organic Chemistry with Centre of Phytochemistry
Ani Petrova
Institute of Organic Chemistry with Centre of Phytochemistry
Petya Dimitrova
Stephan Angeloff Institute of Microbiology
Margarita Kambourova
Stephan Angeloff Institute of Microbiology

Research Article

Keywords: Antarctic yeasts, chemical composition, chromatography, exopolysaccharide synthesis, interferon-gamma, macrophages

Posted Date: May 26th, 2022

DOI: https://doi.org/10.21203/rs.3.rs-1681918/v1

Abstract

The current study aimed to investigate exopolysaccharides (EPSs) produced by two Antarctic yeasts isolated from soil and penguin feathers samples collected on Livingston Island (Antarctica). The strains were identified as belonging to the species *Leucosporidium yakuticum* (LY) and *Cystobasidium ongulense* (CO) based on a molecular genetic analysis. The EPS production was investigated at submerged cultivation. Different chemical, chromatographic, and spectral analyses were employed to characterize EPSs. LY accumulated 5.5g/L biomass and 4.0g/L EPS after 120 h of cultivation, while CO synthesis 2.1g/L EPS at the end of cultivation and biomass amount reached 5.5g/L. LY-EPS was characterized by a higher total carbohydrate content (80%) and a lower protein content (18%) by comparison with CO-EPS (62%, 30%). The LY-EPS mainly consisted of mannose (90 mol%), whereas CO-EPS had also glucose, galactose, and small amounts of uronic acids (8-5 mol%). Spectral analyses (FT-IR and 1D, 2D NMR) revealed that LY-EPS comprised a typical *β*-(1→4)-mannan. Branched (hetero)mannan, together with β/α-glucans constituted the majority of CO-EPS. Unlike LY-EPS, which had a high percentage of high molecular weight populations, CO-EPS displayed a large quantity of lower molecular weight fractions and a higher degree of heterogeneity. LY-EPS (at a concentration of 100 ng/mL) elevated significantly interferon IFN-γ production in splenic murine macrophages and NK cells. The results indicated that newly identified EPS might affect IFN-γ signaling and in turn, might enhance anti-infectious responses. The data obtained also revealed the potential of EPSs and yeasts for practical application in biochemical engineering and biotechnology.

Introduction

In recent years, various scientists have concentrated their efforts on the exploration of the icy desert of Antarctica. This continent offers extreme weather events such as high UV, freezing temperatures, and strong winds to the microorganisms, hence they are forced into having an unusual metabolism that allows them to survive (Buzzini et al. 2014; Martorell et al. 2019). The extreme environmental conditions under which Antarctic yeasts grow and the lack of scientific research on their biosynthetic capabilities open the possibility of isolating new molecules with bioactive properties such as polysaccharides. According to scientific knowledge, it is generally assumed that exopolysaccharides (EPSs) help actively yeasts to adapt to changing extreme environmental conditions. Other scientists share the opinion that EPSs protect the cell from biotic and abiotic stress (temperature, pH, or light intensity) (Donot et al. 2012; Ali et al. 2020). The exploration of the nature of the Antarctic yeast-synthesized EPSs is the subject of previous studies by Pavlova et al. (2009, 2011) and Rusinova-Videva et al. (2011, 2020, 2022). These scientists highlighted the fact that Antarctic yeasts infrequently synthesize pure homo-EPS. On the contrary, they produce hetero-EPSs comprised of mannose, commonly accompanied by glucose, galactose, arabinose, and non-carbohydrate constituents. For example, *Cryptococcus laurentii* AL_{62} strain produced (xylo)mannan composed mainly of xylose and mannose, and a lower amount of glucose (Rusinova-Videva et al. 2011). Interestingly, an uncommon EPS was produced by a soil-inhabited strain *Cryptococcus laurentii* AL_{100}. Its major sugar constituent was arabinose (61%) followed by mannose and

glucose. Very minor constituents were galactose and rhamnose. The structure and composition of EPSs seem to depend on the yeast strains and cultivation conditions used. Furthermore, the results of the physicochemical examination suggested that polymers synthesized by Antarctic yeasts can be used as emulsifiers, stabilizers, and thickeners within the food and cosmetic industry (Pavlova 2014).

A large number of non-Antarctic yeasts produce EPSs (e.g. *β*-glucans, mannans) having prominent biological activities (antioxidant, anti-inflammatory, anti-tumor, immunomodulation). A *Rhodotorula glutinins*-produced EPS is a case in point. Its neutral sugar composition showed that mannose, glucose, and arabinose were the main sugar constituents. This EPS exhibits *in vitro* antioxidant activities, and what is more, it is capable of inhibiting the proliferation of the growth of colon carcinoma HCT-116 cells, and HAV virus (Ghada et al. 2012). Another representative of this genus, *Rhodotorula mucilaginosa* CICC 33013-formed EPS (galactose, glucose, and mannose as main constituents) which exhibited radical scavenging and antitumor activities against human liver cancer cells (Ma et al. 2018). EPSs synthesized by Antarctic yeasts, on the other hand, did not affect the mouse monocyte–macrophage cell line viability and the proliferation of a human breast cancer cell line suggesting high compatibility and low levels of toxicity of these polymers (Poli et al. 2010). It seems that Antarctic yeasts are unique in having the capability for producing EPSs with different useful properties allowing their application in different fields (nutritional, cosmetic, and pharmacological). This is why it is essential to screen more yeast strains that produce EPSs, and to study their physico-chemical and biological features, in order to find a better producer. In spite of this, a large number of yeast genera have not been studied for their potential for biosynthesis of EPSs. Many structural characteristics of EPS constituents are still not investigated in detail. Moreover, very few scientists have focused their attention on careful investigation of the biological effects of yeast-produced EPSs on innate immune cell activation. Therefore, in this study, we decided to concentrate our efforts on the investigation of the capacity of unexplored Antarctic yeasts for synthesizing EPS, to characterize the obtained EPSs, and to identify their biological effects on innate immune cells.

Materials And Methods

Antarctic yeasts

Two morphologically different yeast strains were isolated from soil and penguin feathers samples collected on the territory of the Bulgarian base on Livingston Island (Antarctica). The first strain, AL_{101} was isolated from penguin feathers whereas the second (AL_{102}) was isolated from soil. These strains are stored in Antarctic yeast collection of the Stephan Angeloff Institute of Microbiology, Bulgarian Academy of Sciences. The phylogenetic analysis of ITS1-5. 8S-ITS4 regions of 18S-rRNA revealed that they belonged to *Cystobasidium ingulense* and *Leucosporidium yakuticum* respectively, identification as described in our previous work (Rusinova-Videva et al. 2022). The sequences were deposited in National Center for Biotechnology Information with the numbers SUB11505954 and SUB 11505963, respectively.

Growth medium and cultivation conditions

The LB medium was used for the identification of the isolates. Before sterilizing the medium (20 min, 121°C), its pH was adjusted to 7.5. The solid-phase cultivation was performed at 4°C for 14–20 days. The nutrient medium used for submerged cultivation contained the following ingredients (w/v): 4% sucrose, 0.25% $(NH_4)_2SO_4$, 0.1% KH_2PO_4, 0.05% $MgSO_4 \times 7H_2O$, 0.01% NaCl, 0.01% $CaCl_2 \times 2H_2O$, 0.1% yeast extract (Sigma-Aldrich Chemie, Taufkirchen, Germany). The initial pH of the medium was adjusted to 5.3 and autoclaved for 30 min at 115°C. The fermentation process was conducted in 500 mL flasks on a rotary shaker at 220 rpm, 22°C for 120 h. The inoculum was prepared using the same medium on a rotary shaker at 220 rpm, 22°C for 48 h and it was added in an amount of 10% w/v (Rusinova-Videva et al. 2022).

Determination of the biomass and EPS in the culture medium

The quantification of the biomass and EPS in the culture medium was gravimetrically carried out at the end of the cultivation (120h). In brief, biomass was separated through centrifugation (5000×*g*, 30 min) from the culture suspension. The supernatant was used for the isolation of EPSs through precipitation with 96% ethanol (24h, 4°C). The precipitated EPS was dried at 105°C to a constant weight. Biomass was washed twice with ultrapure water before drying at 105°C until there was no change in its mass.

Isolation of EPSs

Initially, the biomass was separated from the culture suspension by centrifugation at 5000×g for 25 min at 20°C. Afterwards, the volume of supernatant was reduced threefold through a vacuum concentration at 50°C (-0.1MPa). In order to precipitate EPS, 96% (v/v) cold ethanol was added to the concentrated supernatant (1:3 v/v) and the mixture was incubated overnight at 4°C. To recover the precipitate formed during storage centrifugation at 5000×g for 20 min was carried out. The precipitate was further dissolved in ultrapure water and extensively dialyzed (VISKING®, SERVA Electrophoresis, Germany, MWCO 12–14 kDa) against distilled water for 72 h at 4ºC, with a periodic change of water. The dialyzed EPSs were centrifuged at room temperature, filtered through a Büchner funnel, and freeze-dried. The obtained EPSs were named CO-EPS (*C. ongulense*) and LY-EPS (*L. yakuticum*).

General analytical methods

A micro-Kjeldahl method was employed for the estimation of the crude protein content of the EPSs. The quantification of nitrogen expressed as ammonia content of the digested sample was performed by acetylacetone–formaldehyde colorimetric method, using ammonium sulfate as a standard (NFSS 2010). The results were calculated using a nitrogen-to-protein conversion factor of 5.78. The total carbohydrate content of the EPSs was performed by the phenol-sulfuric acid method using mannose as a standard (DuBois et al. 1956). Initially, EPSs were pre-hydrolyzed in 72% (w/w) H_2SO_4 (1 h, at 30°C), and after dilution with water to 1 M H_2SO_4, hydrolysis was completed within the range of 3 h at 100°C in a block heater (Stuart®, SBH200D). The obtained hydrolyzates were used as samples for analysis. The absorbance was measured at 490 nm. A part of the hydrolysate was taken for the analysis of total uronic

acid content. An automated 3-phenylphenol analysis was conducted by a continuous flow analyzer Skalar San^{++} system (Skalar Analytical BV, Breda, the Netherlands), according to the instructions of the manufacturer. Absorption was measured at 530 nm and glucuronic acid (12.5–100.0 µg/mL) was used as a standard. The qualitative estimation of rare sugars was performed by the periodate thiobarbituric acid colorimetric method of Karkhanis et al. (1978) as described by Ognyanov et al. (2018). The acetyl content of EPSs was estimated photometrically by the hydroxamic acid reaction method of McComb & McCready (1957), using β-D-glucose pentaacetate (24–120 µg/mL) as a standard.

Monosaccharide composition analysis

Initially, twenty milligrams of EPS were hydrolyzed with 2 M trifluoroacetic acid (10 mL) for 1.5 h at 121°C in order to release the monosaccharide constituents. Hydrolyzates were vacuum-dried at 40°C and re-dissolved in distilled water. This step was repeated twice to ensure the complete removal of trifluoroacetic acid. Finally, the hydrolyzates (10 mg/mL) were filtered (0.45 µm) and 10 µL were auto-injected into a Nexera-*i* LC2040C Plus UHPLC system (Shimadzu Corporation, Kyoto, Japan), coupled with a Zorbax Carbohydrate column (4.6×150 mm, 5 µm) and Zorbax Reliance Cartridge guard-column operating at 35°C. The samples were eluted with a mobile phase composed of a mixture of acetonitrile/H_2O (80:20 v/v) at a flow rate of 0.6 mL/min. The eluate was monitored using a refractive index detector RID-20A (cell temperature 40°C). The concentration of sugars in the sample was deduced using a calibration curve constructed by plotting the peak area (X-axis) against five different concentrations (Y-axis) for each sugar. The peak corresponding to different sugars in the sample was confirmed by a comparison of retention time with that of the standards.

Molecular weight distribution analysis

Initially, the EPSs (2 mg/mL) were dissolved in distilled water and incubated for 24 h. The molecular weight distribution of EPSs was carried out on a Nexera-*i* LC2040C Plus UHPLC system (Shimadzu Corporation, Kyoto, Japan), coupled with a RID-20A detector, using a Bio SEC-3 column (4.6×300 mm, 300Å, 3 µm, Agilent). Ten microlitres of the filtrated (0.45 µm) solution of the sample were auto-injected and eluted at 30°C with a mobile phase composed of 150 mM NaH_2PO_4 (pH 7.0), employing a flow rate of 0.5 mL/min. Pullulan standards (Shodex standard P-82 kit, Showa Denko, Japan) with molecular weights in the range of 0.59×10^4 to 78.8×10^4 g/mol were used for the construction of a logarithm standard curve.

Fourier transform infrared (FT-IR) spectroscopy

The FT-IR spectra of the EPS samples (2 mg) were recorded in the region 4000 – 500 cm^{-1} using the attenuated total reflection technique on Tenzor 27 (Bruker, Germany), controlled by OPUS 8.7. software. The two spectra were analyzed in Spectragryph software (Friedrich Menges).

Nuclear magnetic resonance (NMR) spectroscopy

EPSs (30 mg) synthesized by LY and CO were dissolved in 700 µL D_2O and lyophilized. After that, polysaccharides were dissolved again in 700 µL D_2O and transferred with Pasteur pipettes into NMR cuvettes. ^{1}H, ^{13}C, DEPT- 135 and $^{13}C/^{1}H$ HSQC, $^{1}H/^{1}H$ COSY, DIPSI, ROESY and $^{13}C/^{1}H$ HMBC spectra were obtained on a Bruker Avance II + 600 spectrometer (Bruker, Germany), equipped with Bruker TopSpin™ software operating at a temperature of 60°C. DSS was used as an internal standard.

Effect Of Exopolysaccharides On Innate Immune Cells

Cell isolation

Spleen was collected from two female Balb/c mice 12 weeks old, weight 18 ± 2 g. The organ was disintegrated in a petri dish through sterile mesh with a pore size of 100 µm (Costar, German). Bone marrow (BM) was isolated by flushing murine femur and tibia with 2 mL sterile phosphate-buffered solution (PBS; pH 7.4). After washing 2 times with PBS (centrifugation 10 min, 250 × g), erythrocytes in cell suspensions were lysed for 5–10 min with 5 mL ACK lysis buffer (150 mM NH_4Cl; 10 mM $KHCO_3$; 0.1 mM Na_2EDTA) pre-warmed at 25°C. Cells were washed 2 times with PBS, counted and resuspended at concentration 2×10^6/mL in RPMI-1640 medium (cat No R8758, containing L-Gln and sodium bicarbonate; Sigma-Aldrich, Germany) supplemented with antibiotics (containing 10.000 U/mL penicillin, 10 mg/mL streptomycin and 25 µg/mL amphotericin B; Sigma-Aldrich, Germany) and 10% fetal calf serum (FBS; heat-inactivated, Sigma-Aldrich, Germany).

Cell culture

Splenocytes or BM cells were added at a concentration of 1×10^6/mL in a volume of 250 µL into a 24-well plate (TPP, Switzerland). The EPS preparations (CO-EPS and LY-EPS), and positive control of LPS (LPS from *Escherichia coli* O55:B5; Sigma Aldrich), and Zymosan (Z4250, Zymosan A from *Saccharomyces cerevisiae*; Sigma Aldrich) were added at volume 250 µL/well at increasing concentrations varied from 100 ng/mL to 100 µg/mL. Cells were cultures for 24 hours at 37°C, 5% CO_2 (Heraeus, Germany). At the last 2 hours of culture, 2 µM monensim sodium salt (Sigma Aldrich) was added at the volume of 100 µL/well to block cytokine secretion.

Flow cytometry analysis

After cell culturing in the presence/absence of the EPS preparations, cells were collected, washed 2 times with PBS, counted, and resuspended at 1×10^5/mL in FACS buffer (PBS, 2% bovine serum albumin, 1 mM ethylenediaminetetraacetic acid (EDTA), 0.1% sodium azide, all from Sigma-Aldrich, Germany). Cells were incubated for 20 min, dark, 4°C with 0.1µg/mL of the following antibodies: anti-CD335 labelled with FITC, anti-TRAIL labelled with PE, anti-F4/80 labelled with PE, anti-TLR24 labelled with PE. Cells were washed 2 times with PBS and then fixed with 4% paraformaldehyde (PFA)/PBS (Biolegend, UK) for 10 min at room temperature. For intracellular flowcytometry, after 2 times washing in PBS, the cells were treated with 500 µL of permeabilization buffer (Biolegend, UK) and incubated for 40 min, dark, 4°C with 0.1 µg/mL. Anti-

IFN-γ antibody labelled with APC or Cy7 (Biolegend, UK). Cells were washed 4 times with PBS and subjected to analysis at a BSR II flow cytometer (Beckton Dickinson, USA) using DIVA 6.0 software (Beckton Dickinson, USA).

Statistics

All cultivations were performed in duplicates. The HPLC analyses were performed at least in duplicates whereas the other analyses were run at least in triplicates. Results were expressed as mean values ± standard deviations. One-way analysis of variance (ANOVA) and Student's *t*-test were used to evaluate the differences in the mean between groups. P values less than 0.05 were considered to be significant. Microsoft Excel, 2016 (Microsoft Corporation, Redmond, USA) was used in the analyses.

Results

Identification and cultivation of yeast strains

Two different strains were identified as *Cystobasidium ongulense* (CO) and *Leucosporidium yakuticum* (LY). They differed in respect of size and morphological characteristics. CO colonies were orange in colour and the cells were elliptical in size of 4.8 × 2.9 µm, while the colonies of LY were characterized by white colour and the cells had a smaller size (3.9 × 2.6 µm) (**Fig. S1 a, b**).

Figure 1 represents the yeast growth, accumulation of EPSs, and the change of pH of the culture medium during the fermentation process. CO followed the standard course of the exponential growth, although it reached slowly the stationary phase after 72 h (**Fig. 1a**). By contrast, LY reached the stationary phase between 48 h and 72 h (**Fig. 1b**). The amount of accumulated biomass reached the highest level of 5.4 g/L and 5.65 g/L at 120th h of cultivation. As can be seen from these figures, the accumulation of biomass was paralleled by an increase in the quantity of EPS till the end of 24 h, but afterward, the accumulation pattern of EPS changed significantly for both species. According to **Fig. 1 a**, the largest quantity of CO-synthesized EPS (2.1 g/L) was determined at 72 h. It is interesting to note that a significant proportion of CO-EPS (> 77%) was actively synthesized during the first 24 hours of cultivation. Until the end of cultivation, its amount decreased by 38%, but this did not change the course of yeast growth. It may be that the initially synthesized EPS was metabolized by CO, and the released constituents were used further for supporting and activating cell growth. This is quite possibly caused by the exhaustion of easily available carbon sources. As regards LY, a higher amount of EPS (4.0-4.5 g/L) was accumulated at a later stage of cultivation (96-120th h), although a higher proportion of EPS was formed up to 24th h (> 66%) (**Fig. 1 b**). Interestingly, after a short period of stagnation (24-55 h), the content of EPS increased smoothly till the end of the cultivation process. However, this period was accompanied by excessive yeast growth. After starting the cultivation, pH began to decrease from 5.3 to 2.0 for 48h. Sharp pH decrease was observed in the first 24h for rapidly growing LY, while the CO's development caused the pH value to fall slowly to its lowest level for 48 h.

[Figure 1]

Chemical characterization of EPSs

The yield of EPSs is shown in **Table 1**, where monosaccharide composition and other chemical characteristics are included. As can be seen, LY seemed to be a better producer of EPS in comparison with CO strain. Interestingly, three times as much EPS was formed by LY as CO for the same period of cultivation (120 h). The total carbohydrate content of LY-formed EPS represented a larger proportion of the dry matter content (80%), while the other producer accumulated polymer characterized by a lower amount of carbohydrates (62%). An interesting finding of the study was that protein constituted an appreciable amount of CO-formed polymer (30%). By contrast, LY-EPS was accompanied by a smaller amount of protein (18%). It seems that the investigated EPSs were of neutral type because neutral sugars accounted for 66% (w/w) and more of the total sugar content, while acidic components did not exceed 6% (w/w). Next to mannose (30% w/w), CO-EPS was also composed of glucose, galactose, and minor quantities of uronic acids suggesting that this polymer was of hetero-mannan type. Compared to CO-EPS, LY-EPS was found to be highly enriched in mannose which may be accounted for the presence of a mannan-type PS. This sugar made up nearly 95% of total neutral sugars, whereas the uronide-containing components were found in a fairly low percentage. As can be seen, EPSs tested negative for rare sugars, because a less typical orange colour was observed. It is interesting to note that some sugar residues that constituted EPS were *O*-acetylated to a different extent. Acetyl groups were found in a low amount in LY-EPS, but they were present in a much higher amount in CO-EPS. **[Table 1]**

Molecular weight distribution of EPSs

To estimate the molecular weight distribution of EPSs, an HPSEC analysis was employed and the resulting elution profiles are shown in **Fig. 2**. The presence of high molecular weight fragments in LY-EPS, eluted in the range of RT 5.0 and 7.0 min, was recognized (**Fig. 2 a**). The main peak covered the mass range between > 47 × 10^4 g/mol and 70 × 10^4 g/mol. It is easy to be calculated that the high molecular weight populations (RT 5.5–7.0 min) occupied a higher percentage (64%) of the total (100%) peak area, thus a large percentage of EPS. As shown in **Fig. 2 a**, a small amount of EPS fraction (26%), covering a mass range between 10 × 10^4 g/mol and 1 × 10^4 g/mol, were eluted at an RT of 7.5 – 10 min. As regards the CO-EPS elution pattern, remarkable differences can be seen. CO-EPS consisted of two distinct populations with different distributions of molecular weights and higher heterogeneity. The first main fraction which comprised about 28% of the total peak area (100%), and therefore a smaller percentage of EPS, were eluted early between 5.5 and 7.5 min. It covered the mass range of 78×10^4 and 21×10^4 g/mol. Next to those populations, a second main peak, which represented fractions composed of lower molecular weight fragments, was eluted (RT 8.5 – 11.0 min). Different peaks covered the range of 11.2×10^4 and 1.2×10^4 g/mol occupying 3%, 8%, and 61% of the total peak area suggesting that a large quantity of lower molecular weight fractions was present.

[Figure 2]

FT-IR spectroscopy of EPSs

The FT-IR spectrum of LY-EPS and CO-EPS are shown in **Fig. 3**. It was very clear that spectra were typical for polysaccharides because a band at about 3300 cm^{-1} and two bands at about 2900 cm^{-1}, assigned to O—H, C—H, and C—H_2 stretching, were observed. However, the band at 3340 cm^{-1} due to O—H stretching could not be distinguished from that showing N—H stretching (hydrogen-bonded N—H_2 group). Bearing in mind a higher protein content present in EPSs, several bands can be assigned to the amide group vibrations. The bands at 1542 and 1638 cm^{-1} were assigned for δ(N—H) and ν(C—N) of amide II and N-linked C=O of amide I structure vibrations (Hamidi et al. 2020). The absorption bands at 1638 and 1411 cm^{-1} could be also attributed to $\delta_s(CH_2)$ and $\delta_s(CH_3)$ of proteins rather than the ionized carboxyl groups of uronic acids because they were found in smaller amounts (Synytsya et al. 2003). The C=O stretching vibration of the *O*-acetyl group (ester) and $\tau(CH_2)$ gave rise to absorption at 1246 cm^{-1} together with a weak band at 1720 cm^{-1}. Moreover, bands at 1246 and 1312 cm^{-1} may be caused by amide III vibrations (δ(N—H) and ν(C—N)) of protein components. The band at 1375 cm^{-1}, in general, assigned to the C—H bending vibration of CH_3 group and $\omega(CH_2)$, may originate from C—H vibrations in monosaccharide residues. The presence of bands at 1151 cm^{-1} and 1061 cm^{-1} corresponded to O—C—O, C—O, and C—C stretching of glycosidic bond vibration of mannose-containing polysaccharides. Other bands encountered with mannan-type PS were: 1024, 943, and very specific signals at 872 and near 807 cm^{-1} which could be assigned to C—O, C—C stretching, C1—H bending, and ring vibration (C—O, C—C) of monosaccharide rings. Further, the IR-FT spectrum showed the presence of bands for β-anomer configurations (β-C—O—H, β-C—C—H, β-C—O—C, β-C—C—O, β-O—C—O) of the monosaccharide units (1023, 943, about 900, 872, 806, and 742 cm^{-1}). What is more, in accordance with Kato's findings (Kato et al. 1973), bands at 742, 940, and 1152 cm^{-1} could be associated with the glycosidic bond vibrations of manno-pyranosyl units having β-(1→4) glycosidic linkage. On the basis of chemical composition and FT-IR spectral analysis, it can be supposed that LY-EPS comprised a typical β-mannan PS. CO-EPS, on the other hand, seemed to be hetero-mannan and β-glucan PSs.

[**Figure 3**]

NMR spectroscopy of EPSs

To give more precise details about the structure of LY-EPS and CO-EPS, several 1D and 2D NMR experiments were carried out. The identified structural fragments are presented in **Table 2**, and their HSQC spectra are shown in **Fig 4**. ^1H spectrum of LY-EPS contained two major anomeric signals with similar intensity at δ 4.85 and 4.72 ppm, which correlated with the signals at δ 97.6 and 100.7 ppm in the HSQC spectrum, respectively. Using specific correlations in the COSY, DIPSI, ROESY, and HMBC spectra, it was found that these peaks derived from substituted β-mannopyranosyl units. In addition, intense intra-residue resonances between H-1 (4.85 ppm) with H-2 (4.12 ppm) and H5 (3.51 ppm) or a transglycosidic interaction H-1/H-4 (4.85/3.85 ppm) of 1,4-β-D-Man*p* residues were observed in the ROESY spectrum. Moreover, high-intensity cross-peaks between H-1 (4.72 ppm) with H-2 (4.23 ppm), H-3 (3.93 ppm), H-4

(3.85 ppm), or H-5 (3.47 ppm) of the other 1,3,4-*β*-D-Man*p* residues were also found in the same spectrum (Makarova et al., 2018).

[**Figure 4**]

Furthermore, intense through-bond couplings at 100.7/3.85 ppm and 77.4/4.72 ppm, together with a low-intensity cross-peak at 100.7/3.47 ppm attributed to C-1/H-4, C-4/H-1 and C1/H5 of 1,3,4-*β*-D-Man*p* units were registered in the HMBC spectrum. Therefore, it was confirmed that LY-EPS was mainly composed of *β*-(1→4)-mannan.

[Table 2]

Interestingly, the movement of the chemical shift of C-3 (79.9 ppm) of one of the identified 1,4-*β*-D-Man*p* residues in the downfield region indicated the presence of *O*-3 substitution of this monomer. Firstly, it was hypothesized that 1,4-*β*-D-Man*p* formed a homomannan branched at *O*-3 with another Man residue because of the intense cross-peak at 79.9/4.85 ppm between C-3 of 1,3,4-*β*-D-Man*p* and H-1 of 1,4-*β*-D-Man*p* in the HMBC spectrum. Additionally, the existence of two cross-peaks at 4.85/3.93 ppm and 4.85/4.23 ppm between H-1 of 1,4-*β*-D-Man*p* with H-2 and H-3 of 1,3,4-*β*-D-Man*p* in the ROESY spectrum supported this hypothesis. The ratio between the integral intensities of H-1 (4.72 ppm) of 1,3,4-*β*-D-Man*p* and H-1 (4.85 ppm) of 1,4-*β*-D-Man*p* was 51:49, which revealed that nearly half of Man residues were *O*-3 substituted. Secondly, an intense through-bond resonance between the signal at 97.7 ppm of C-1 of 1,4-*β*-D-Man*p* units and the peak at 4.97 ppm was detected in the HMBC spectrum. It was elucidated that the anomeric signal at 4.97 ppm originated from terminal *α*-L-Fuc*p* because of the important cross-peak at 98.2/4.97 ppm in the HSQC spectrum and the correlation between the signal at 4.97 ppm and that at 3.71 ppm in the COSY spectrum, and specific correlations in the DIPSI spectrum (Li et al. 2016; Chen et al. 2021). It was found that some of the 1,4-*β*-D-Man*p* residues were *O*-3 substituted with *α*-L-Fuc*p*, which was supported by the through-space internuclear spin–spin couplings at 4.97/4.23 and 4.97/3.93 ppm between H-1 of *α*-L-Fuc*p* and H-2 and H-3 of 1,3,4-*β*-D-Man*p* in the ROESY spectrum. This explained the long-distance four-bond correlation at 97.7/4.97 ppm in the HMBC spectrum. A high ratio of the integral intensities of H-1 of 1,3,4-*β*-D-Man*p* to H-1 of *α*-L-Fuc*p* (95:5) suggested that a very small percentage of Man residues was Fuc-substituted.

Additionally, correlations between the proton and carbon from the CH_3 group of acetyl esters at 2.16-2.20/21.1 ppm were found in the HSQC spectrum (**Fig. 5**). The C=O signal of the acetyl esters resonating at 174.4 ppm was determined from the HMBC spectrum. It was speculated that acetyl groups were localized at *O*-2 and/or *O*-3 of Man residues, as it has already been found in different *β*-glucomannans (Hannuksela et al. 2004; Makarova et al. 2018). Apart from that, the minor signals at 4.59 and 4.51 ppm were attributed to H-1 of Xyl, which was found to be terminal linked, according to specific correlations in COSY, DIPSI, ROESY, and HSQC spectra, most probably attached to *β*-D-Man*p* (Makarova et al. 2013; Shakhmatov & Makarova 2022).

[Figure 5]

As regards CO-EPS, fairly complex spectra (^{1}H and ^{13}C) were observed most probably due to the difference in the composition. Similar to LY-EPS, using specific correlations in the HMBC and ROESY spectra, it was found that CO-EPS also contained 1,4- and 1,3,4-*β*-D-Man*p* fragments (**Table 3**). It was shown that *O*-3 substitution of 1,4-*β*-D-Man*p* residues was dominated by Man, but cross-peaks between H-1 (4.91 ppm) of *α*-L-Fuc*p* with H-2 (4.24 ppm) and H-3 (3.93 ppm) of 1,3,4-*β*-D-Man*p* were also found in the COSY and ROESY spectra. The presence of *α*-L-Fuc*p* in CO-EPS was observed by the correlations at 1.27/18.3, 4.91/100.0, and 69.8/4.27 ppm, attributed to H-6/C-6, H-1/C-1, and H-5/C-5 in the HSQC spectrum (Li et al., 2016). In the COSY spectrum, the resonances between the adjacent H-1/H-2 (4.91/3.80 ppm) and H-5/H6 (4.27/1.27 ppm) also showed that the sample contained a terminal linked *α*-L-Fuc*p* residue (Nandi et al., 2013). Therefore, it is reasonable to assume the existence of *O*-3 fucosylated Man units in the EPS sample. Moreover, it was possible to deduce from a specific coupling for CH_3 of the acetyl group at 21.0 and 2.12 or 2.16 ppm in the HSQC spectrum that CO-EPS was acetylated. Two correlations between the carbonyl group and methyl proton of acetyl esters were detected at 174.3/2.12 ppm and 174.8/2.16 ppm in the HMBC spectrum, revealing the existence of at least two different ester substitution patterns. Furthermore, it was demonstrated that methyl protons (2.12-2.16 ppm) of acetyl groups interacted through space with the signals at 3.53 and 4.73 ppm (low-intensity) in the ROESY spectrum, which showed that Man was acetylated. Additionally, two cross-peaks at 2.12-2.16/5.03 (low-intensity) and 2.12-2.16/4.14 ppm in the ROESY spectrum confirmed that *β*-1,4-D-Man*p* was *O*-3 acetylated. This was also supported by the low-intensity coupling between the signal at 174.3 for C=O group and this at 4.14 ppm for H-2 of *β*-1,4-D-Man*p* in the HMBC spectrum. Using correlations in the COSY, DIPSI, ROESY, and HSQC spectra, all protons, and carbons in the residue →4)-*β*-Man*p*-3-*O*Ac-(1→ were assigned (Hannuksela et al. 2004; Zhang et al. 2022).

[Table 3]

Furthermore, it was demonstrated that CO-EPS contained not only *β*-mannan fragments but also *α*-mannan structures (**Table 3**). This was supported by the observation that 1,2-*α*-D-Man*p* residues had the following through-bond resonances at *δ* 5.07/79.0 ppm and 5.05/83.7 ppm in the HMBC spectrum for H-1 of a terminal *α*-D-Man*p* unit or H-1 of 1,2-*α*-D-Man*p* with C-2 of 1,2-*α*-D-Man*p* and between H-1 of *α*-Man*p*-(1,2) with H-2 of 1,2(,6)-*α*-D-Man*p*, respectively (Galinari et al. 2017; Ustyuzhanina et al. 2018). Similarly, the following important two through-space internuclear spin–spin couplings were observed in the ROESY spectrum between H-1 of *α*-Man*p*-(1→2) and H-2 of 1,2-*α*-D-Man*p* (5.05/4.07 ppm), and between H-1 of 1,2,6-*α*-D-Man*p* and H-2 of 1,2-*α*-D-Man*p* (5.11/4.07 ppm) (Ustyuzhanina et al. 2018). Additionally, specific interactions between 5.09/70.9 ppm for H-1 of *α*-D-Man*p* and C-3 of 1,2(,6)-*α*-D-Man*p* or 5.11/101.1 ppm for H-1 of 1,2,6-*α*-D-Man*p* and C-1 of 1,2-*α*-D-Man*p* in the HMBC spectrum confirmed *O*-2 homomannan substitution pattern. On the other hand, a low-intensity coupling was registered between H-1 (5.11 ppm) and C-6 (66.5 ppm) of 1,2,6-*α*-D-Man*p* in the HMBC spectrum, confirming the existence of 1,6-linked *α*-D-Man*p* units (Tang et al., 2022). This was also observed in the ROESY spectrum by the cross-peaks H-1/H-6 (5.11/4.02 ppm) and H-1/H6’ (5.11/3.77 ppm) of 1,2,6-*α*-Man*p*. The low-intensity correlation peaks at 5.07/78.0 and 4.07/81.9 ppm in the HMBC spectrum, as

well as the resonances at 4.11/81.9 and 4.07/78.0 ppm in the HSQC spectrum, showed the presence of 1,2,3-linked *α*-D-Man*p* units (Zhang et al. 2021). It is probably safe to assume that 1,2(,3),6-*α*-D-homomannan regions constituted CO-EPS. On the other hand, a low-intensity correlation was observed between C-1 (102.7 ppm) of 1,2-, 1,2,3- and 1,2,6-linked *α*-D-Man*p* and anomeric proton (4.91 ppm) of *α*-L-Fuc*p*. Therefore, it was hypothesized that *α*-L-Fuc*p* could be found attached to *α*-D-mannans. The cyclic hemiacetal pyranose form of *α*-D-Man*p* in CO-EPS was revealed by the specific H-1/C-5 couplings at *δ* 5.07/73.8, 5.25/73.8, 5.11/73.8, 5.05/73.8 ppm for terminal, 1,2-*α*-D-Man*p*, 1,2,6-*α*-D-Man*p,* and *α*-D-Man*p*-(1→2) residues. It should be noted that the presence of phosphorylated or *O*-3 methylated *α*/*β*-D-Man*p* units can be excluded (Suárez et al. 2010), but other constituents of the CO-EPS seemed to bear *O*-methyl groups because of the cross-peak at *δ* 3.46/57.0 ppm in the HSQC spectrum. The specific intra-residue resonance at 3.46/80.4 ppm was observed in the HMBC spectrum. The carbon at 80.4 ppm was coupled with the proton at 3.53 ppm in the HSQC spectrum. The proton of methyl group at 3.44 ppm resonated with the following adjacent protons at 3.53, 3.88, and 4.30 ppm in the ROESY spectrum, which were assigned to H-3, H-2, and H-4 of 1,6-linked 3-*O*-Me-*α*-D-Gal*p* (Ellefsen et al. 2021; Komura et al. 2010). The presence of 1,6-*α*-D-Gal*p* units was observed in the ROESY spectrum by the long-distance internuclear spin-spin correlation peaks at 4.96/3.69, 4.96/3.90, and 4.96/4.20 ppm for H-1/H-6, H-1/H-6’ and H-1/H-5, respectively (Komura et al. 2010; Samuelsen et al. 2019). The same information was also found for *O*-3-methylated 1,6-*α*-D-Gal*p*. Additionally, low-intensity couplings between H-1 (4.96 ppm) with C-6 (67.2 ppm), and C-5 (69.5 ppm) of 1,6-linked *α*-D-Gal*p* or between C-1 (98.6 ppm) and H-6 (3.69 ppm) of the same residue were detected in the HMBC spectrum. Using specific interactions in the COSY, HSQC and DIPSI spectra 1,2,6-linked *α*-D-Gal*p* units were elucidated (Ellefsen et al. 2021). It could be argued that Gal constituents of CO-EPS were *O*-2 substituted by *α*-L-Fuc*p* as Nandi et al. (2013) has noted. Interactions between H-1 (4.91 ppm) of a terminal *α*-L-Fuc*p* unit, H-2 (3.96 ppm), and H-3 (4.02 ppm) of 1,2,6-*α*-D-Gal*p* in the ROESY spectrum were observed, which revealed that 1,6-linked *α*-D-Gal*p* was partly *O*-2 substituted by *α*-L-Fuc*p*. However, CO-EPS was characterized by a low Fuc content, hence it was hypothesized that *α*/*β*-D-Man*p* was also positioned at *O*-2 to some of the 1,6-linked *α*-D-Gal*p* residues. Indeed, a correlation peak was detected between H-1 (5.07 ppm) of *α*-D-Man*p* and C-2 (80.4 ppm) of 1,2,6-*α*-D-Gal*p* in the HMBC spectrum. Additionally, in the same spectrum was found a cross-peak at 5.11/98.6 ppm, which was supposed to be a result of an interaction between H-1 of 1,2,6-*α*-D-Man*p* and C-1 of 1,2,6-*α*-D-Gal*p*, although the signal at 5.11 ppm also belonged to the anomeric proton of this Gal residue. Similarly, a specific coupling at 5.07/3.96 ppm was attributed to inter-residue interaction between H-1 (5.07 ppm) of *α*-D-Man*p* units and H-2 (3.96 ppm) of 1,2,6-*α*-D-Gal*p* residues in the ROESY spectrum. Furthermore, the correlation peak at 4.65/105.2 ppm in the HSQC spectrum, in addition to the signal at 4.65/3.58 ppm in the COSY spectrum were attributed to H-1/C-1 and H-1/H-2 of 1,4-*β*-D-Gal*p* structures (Naumenko et al. 2018; Previato et al. 2019). The existence of 1,4-linked *β*-D-Gal*p* was confirmed by the interactions between H-1 (4.65 ppm) and C-4 (80.4 ppm), and H-1 (4.65 ppm) and H-4 (4.02 ppm) in the HMBC and ROESY spectra, respectively.

Furthermore, it was found that Glc in CO-EPS was terminal, 1,3-, 1,6- and 1,3,6-linked in *β*-anomeric configuration and 1,4-linked in *α*-anomeric configuration. This was suggested by the correlation peaks at

4.73/103.3, 4.78/103.3 (low-intensity), 4.53/103.3, 4.57/103.1, and 5.36/99.5 ppm, respectively in the HSQC spectrum (Aimanianda et al. 2009; Samuelsen et al. 2019; Huo et al. 2020; Ellefsen et al. 2021). The couplings at 4.73/85.1 ppm between H-1 of terminal *β*-D-Glc*p* units and C-3 of 1,3-*β*-D-Glc*p* units or between C-1 (103.3 ppm) of terminal *β*-D-Glc*p* and H-3 of 1,3-*β*-D-Glc*p* in the HMBC spectrum demonstrated the presence of 1,3-linked *β*-D-Glc*p*. This was also confirmed by the interactions between H1 (4.73 ppm) of *β*-D-Glc*p*-(1→ with H-2 (3.56 ppm) and H-3 (3.72 ppm) of 1,3-*β*-D-Glc*p* units in the ROESY spectrum (Aimanianda et al. 2009; Samuelsen et al. 2019). Similarly, it was shown that H-1 (4.53 ppm), H-5 (3.69 ppm), and H-6, 6' (4.20, 3.86 ppm) of 1,6-*β*-D-Glc*p* formed cross-peaks in the ROESY spectrum (Ellefsen et al. 2021). The correlation peak at 4.57/3.53 ppm in the COSY spectrum, together with the correlations for the signal at 4.57 ppm in the DIPSI spectrum, and the resonances at 4.57/3.77 ppm (H-1/H-3) and 4.57/3.86 ppm (H-1/H-6') in the ROESY spectrum demonstrated the existence of 1,3,6-*β*-D-Glc*p* residues (Ellefsen et al. 2021). Moreover, a 1,4-*α*-D-Glc*p* fragment was proven by the adjacent proton interaction at 5.36/3.58 ppm in the COSY spectrum for H-1/H-2 of this structural unit, as well as by the correlation peak at 5.36/3.64 ppm for H-1/H-4 in the ROESY spectrum (Huo et al. 2020). It was also suggested that CO-EPS contained terminal and 1,5-*α*-L-Ara*f* from the correlation peaks at 5.21/109.7, 5.27/107.7, and 5.05/108 ppm, respectively in the HSQC spectrum and from other specific correlations in the COSY, DIPSI and ROESY spectra (Saeed et al. 2018; Shakhmatov & Makarova 2022).

LY-EPS and CO-EPS were studied by 2D NMR spectroscopy. All identified structural fragments in LY-EPS are presented in Table 2. The HSQC spectrum of LY-EPS is shown in **Fig 4**. Additionally, ^{1}H and ^{13}C spectra of LY-EPS are included in Fig. S2 and S3. All identified structural fragments in CO-EPS are presented in **Table 3**. The HSQC spectrum of CO-EPS is shown in **Fig 5**. Additionally, ^{1}H and ^{13}C spectra of CO-EPS are included in **Fig. S4** and **S5**.

Additionally, there were some signals in the range of 0.8 and 3.0 ppm in the ^{1}H spectrum of CO-EPS, which were typical for the protons of the N-H and N-CH_3 groups of proteins. This result was generally consistent with the higher protein content of the sample (**Table 1**). On the basis of the NMR experiments, it can be concluded that CO-EPS is composed mainly of *β*-1,3,4-D-(homo)mannans, *α*-1,2,6-D-(homo)mannans, *α*-(L-fuco)-D-manno-2-(1,6)-galactans, *β*-1,3,6-D-glucans, and *α*-D-glucans.

Biological effect of exopolysaccharides on innate immune cells

The biological effect of EPS solutions on innate immune cells was evaluated. In BM Ly6C+ cells are monocytes with origin of granulocyte precursors. It was used two cell populations as a source of innate immune cells: bone marrow and spleen. In BM we identified monocytes with origin of granulocyte precursors as Ly6C+ cells. In spleen we followed the effect of EPS on macrophages positive for F4/80 and on NK cells positive for CD335. The intracellular level of TNF-α in BM monocytes stimulated in the presence of the EPS preparations and two strong activators Zymosan (TLR2 agonist) and LPS (TLR4 agonist) was determined. Unstimulated monocytes (control group) showed the highest percent of TNF-α positive cells in comparison to all groups treated with preparations, LPS or Zymosan (**Fig. 4a**) indicative for significant TNF-α storage. The stimulation with Zymosan, TLR2 agonist, reduced the intracellular

amount of the cytokine in a dose-dependent manner, and thus we observed the decrease in the TNF-α positive cells. We suggest that the cytokine can be secreted by the intracellular stores during the stimulation period of 24 hours (a period when the cytokine secretion was unblocked by monensim) and thus the number of cells positive for the cytokine was reduced. The effect of LPS was stronger than that of Zymosan showing the depletion of TNF-α positive cells. We observed that all EPS solutions significantly reduced TNF-α positive monocytes even at concentrations of 100 ng/ml and by comparison to the strong activator of TNF-α release -LPS.

[Figure 6]

F4/80 is a marker for tissue-resident macrophages. Tissue macrophages had an important role in the regulation of granulopoieses in BM and emergency granulopoiesis in organs during acute inflammation or tumor growth. It was observed that the percentage of TNF-α positive splenic macrophages was higher in the control group and in the group treated with 100 μg/mL LPS (**Fig. 4b**). Probably in macrophages the high concentration of LPS induced tolerogenic signals and less TNF-α was released. TNF-α positive cells were higher in the group treated with 100 ng/ml of LY-EPS in comparison to groups treated with the same concentration of CO-EPS solution. These data suggest that either LY-EPS prevented TNF-α release by macrophages or it induced *de novo* synthesis of the cytokine that fulfills the depleted intracellular store of the cytokine.

It next evaluated the effect of EPS preparations on IFN-γ production in macrophages (**Fig.4c**). It was observed that LY-EPS increased IFN-γ production in a dose-dependent manner. At the lowest concentration of 100 ng/mL LY-EPS elevated significantly the percentage of IFN-γ producing cells. It has been shown that NK cells expressing a variety of innate receptors might be sensitive to EPS. Thus, we isolated splenocytes and stimulated them for 24 hours with EPS and LPS. It has been shown that LPS can induce IFN-γ production in human NK cells (Kanevskiy et al. 2013). The data showed that LPS can induce IFN-γ production in murine NK cells. It was found that a low concentration of LY-EPS increased significantly IFN-γ production as higher concentrations of LPS. The other EPS solution failed to affect IFN-γ production (**Fig.4d**).

EPSs might affect TLRs expression. TLR2 is an innate receptor that interacts with a diverse range of microbial pathogen-associated molecular patterns (PAMPs) from Gram-positive and Gram-negative bacteria as well as fungi, parasites, and viruses. These PAMPs include cell-wall components, such as lipoproteins, lipoteichoic acid (LTA; Gram-positive bacteria only), lipoarabinomannan (mycobacteria only), and Zymosan (yeasts). TLR2 can be also a ligand for EPS from *Lactobacillus rhamnosus* GG that can alleviate the adipocyte functions (Zhang et al. 2016). EPS from *Lactobacillus plantarum* can induce apoptosis via engagement of TLR2 and further induction of FAS/FASL apoptosis (Zhou et al. 2017). Thus, we have investigated the level of TLR2 on monocytes after treatment with EPS solutions. Zymosan at a low dose induced the expression of TLR2 but at high dose it decreased TLR2 probably because it induces internalization of the receptor. We observed that none of the EPS solutions was able to induce TLR2 expression similarly to LPS (**Fig. 4e**). The transmembrane protein TRAIL was shown to be

able to induce apoptosis in tumor cells (Wiley et al., 1995). We observed that its expression levels after treatment with LY-EPS in 10 µg/mL and CO-EPS in 100 ng/mL and 100 µg/mL were higher than those in the control (**Fig. 4f**).

Discussion

The current study was primarily concerned with an investigation of two yeast strains collected in Livingston Island (Antarctica) and getting information about the production and chemical characteristics of EPS. In addition, our study contributes to scientists' knowledge because there are huge gaps in knowledge concerning EPS producers as far as we know. According to our investigation, yeast producers were identified as CO and LY, respectively. CO was described for the first time as a soil inhabitant isolated from East Angle Island (Antarctica) in 2017, although other species of this genus have also been found in high mountainous parts of China and Italy. It has been reported as a sucrose-consuming strain that can produce valuable enzymes (esterase, lipase, and *β*-glucosidase) (Tsuji et al. 2017). LY, also known as *Rhodotorula yakutica* and *Leucosporidiella yakutica*, was described for the first time by Li et al. (2020). Species of *Leucosporidium*'s genus have been found in permafrost in Antarctica (Vishniac 2006). *L. antarcticum* is known to synthesize proteinase and cold-active glucosidase and *β*-fructofuranosidase (Turkiewicz et al. 2003, 2005). However, with the exception of earlier findings about EPS-synthesizing *L. scottii* (Rusinova-Videva et al. 2019), we did not find any other reports on EPS from another genus member. Both yeast producers have not been studied for their ability to synthesize EPS. The optimal production of EPS was conducted by submerged intensive cultivation. This type of cultivation was preferred to solid-phase cultivation due to a higher yield, takes less time, and much easier separation of biomass and biopolymer (Debnath et al. 2021). Several reports have been previously published on the subject of the cultivation of Antarctic yeasts employing sucrose as a carbon source (Pavlova et al. 2011; Rusinova-Videva et al. 2020, 2022). For example, *Cryptococcus laurentii* AL_{65} has accumulated a greater amount of biomass (7.0 g/L) by comparison with LY and CO (4–5 g/L). However, another yeast strain (*C. laurentii* AL_{100}) cultivated on a sucrose-containing medium has formed not more than 3 g/L biomass. Concerning EPSs, CO-EPS yielded the lowest amount of EPS (2.1 g/L at 48 h) in comparison with LY-EPS (4.5 g/L), although it accumulated higher biomass. However, this yield was comparable to the yield of EPS produced by the *C. laurentii* AL_{65} (3 g/L at 48 h) strain cultivated on a sucrose-containing (2%) culture medium (Pavlova et al. 2011). It is interesting to note that LY-EPS was comparable in yield of EPSs formed by other soil-inhabited producers such as *Vishniacozyma victoriae* and *Tremellomycetes* sp. (4.0-4.5 g/L) (Rusinova-Videva et al. 2022). On the other hand, CO – an inhabitant of penguin feathers, did not bear comparison with them. Therefore, the answer seems to lie mainly in the differences in the metabolism of yeasts, carbon source, and cultivation conditions. Further, our current findings about the decrease in pH during the first hours of cultivation were in complete agreement with previous studies (Pavlova et al. 2004). It gives yeast strains a competitive advantage over other microorganisms sensitive to lower pH.

It is important to remember that the chemical composition and molecular weight distribution of yeast EPSs are considered essential for the explanation of the biological activity and functional properties. This study found that both EPSs were rich in mannose and protein. Moreover, spectral analyses revealed that LY-EPS was formed mostly of *β*-(1→4)-mannans accompanied by protein (e.g. mannoprotein), whereas CO secreted into the culture medium EPS comprised mainly of a mixture of hetero-mannans, *β*-glucan, and protein (e.g. a galactoglucomannan protein fraction). It is a well-documented fact that carbohydrate polymers such as glucans, mannans, chitin, together with lipids and proteins were major constituents of yeast cell walls (Liu et al. 2021). However, it should be mentioned that there is a wide variety of EPSs characterized by different compositions depending on the yeast strain and the composition of the culture medium. By way of example, *Sporidiobolus pararoseus* JD-2- excreted EPS is composed of galactose, glucose, and mannose having a ratio between them of 16:8:1. Uronic acids were not present in the EPS produced by that yeast strain (Han et al. 2018). In our recent study, on the other hand, *Vishniacozyma victoriae* and *Tremellomycetes* sp.-derived EPSs were found to be composed mainly of mannose (37 mol%), while galactose and uronic acids occured in smaller amounts (Rusinova-Videva et al. 2022). Moreover, an earlier study showed that *Sporobolomyces salmonicolor* AL_1 strain produced EPS consisted not only of mannose (43%) and glucose (54%) but also of a small amount of fucose (3.3%). It is interesting to note that EPS composition could be changed when yeast cells are cultivated under stress conditions. For example, the basic sugar constituents of EPS produced by *Cryptococcus laurentii* under salt-stress conditions were mannose, xylose, and galactose in the proportion of 10:6.1:1.1, while the EPS formed under optimal conditions was characterized by a molar ratio of 10:3.4:1.3 (Breierová et al. 2005). It is worth mentioning that CO-EPS and to a greater extent LY-EPS contained acetyl groups which was in line with previously reported findings about an acetylated hetero-mannan (3–10%) (Van Bogaert et al. 2009).

A review of the scientific literature on the topic showed that a diversity of glycosidic linkage compositions of EPS exist. For example, some fungal and yeast *α*-1,6-mannans were branched at *O*-2 with several *α*-D-Man*p* residues, which could be additionally substituted at *O*-3 with terminal *α*-D-Man*p* units (Gómez-Miranda et al. 2004; Galinari et al. 2017). Interestingly, Matsuo et al. (2000) have isolated antigenic acetylated 1,3,4-*β*-D-homomannan from *Leptospira biflexa*, as they have proven *O*-3 substitution with Man by 2D NMR, GC-MS methylation analysis of the glycosidic linkage type and Smith degradation.

Indeed, Yamada et al. (1982) have isolated acetylated fucomannan from the fungus *Absidia cylindrospora* composed of *α*-1,6-mannan branched at *O*-3 with *α*-L-Fuc*p*, thus our study revealed that *β*-1,4-mannans can be also substituted with Fuc.

CO-EPS contained 1,2(,3),6-α-D-homomannan regions, which has already been reported in polysaccharides of many yeast species, such as cell wall polysaccharides from *Pichia pastoris*, *Saccharomyces sp. (e.g. cerevisiae) Candida albicans*, *Kluyveromyces marxianus* and *Candida zeylanoides*, but also in exopolysaccharides from *Kuraishia capsulate* (Gorin et al. 1968; Gorin 1973; Shibata et al. 1995; Kobayashi al. 2013; Galinari et al. 2017; Ustyuzhanina et al. 2018). Interestingly, a 1,2,6-*α*-D-homomannan-type EPS was described to be formed not only by Antarctic yeasts but also by

Antarctic bacterium *Pseudoalteromonas haloplanktis* TAC 125 and Arctic *Sphingobacterium* sp. IITKGP-BTPF3 (Corsaro 2004; Chatterjee et al. 2018). This polymer has also expressed *in vitro* immunomodulatory activity against murine macrophages with anti-inflammatory potential (Chatterjee et al. 2018).

The unique properties of microbial polysaccharides determine the possibility of their use for nutritional, cosmetic, and pharmacological applications in the role of immunostimulants, antitumor, and antioxidant drugs (Freitas et al. 2011; Ghada et al. 2012; Ma et al. 2018; Ragavan and Das 2019; Seveiri Mirzaei et al. 2019; Hao et al. 2020; Hristova et al. 2021). Polysaccharides diversity in terms of species, chain length, molecular weight, and conformation of monosaccharide residues was crucial for the diversity in their biological role (Yang and Zhang 2009; Zhou et al. 2019). Some of the β-glucans are known as biological response modifiers (Leung et al. 2006). β-glucans bind to innate immune receptors triggering immune cell activation and further development of immune responses (Murphy et al. 2010). In addition to the ability to stimulate immune functions some β-glucans also had antioxidant capacity, as was demonstrated in *Cystobasidium benthicum* (Reyes-Becerril et al. 2011). The data have showed that the bioactive β-glucan conjugated with peptide was considered an effective polymeric immunostimulant and antigenic carrier used *in vitro* in Balb/c mouse splenocytes (Sanchez et al. 2021).

Knowledge of the biological activity of exopolysaccharides synthesized by Antarctic yeast was lacking. In view of the expected immunological activity, our research focused on the effect of EPS on innate immune cells. We concluded that either EPS affects other TLRs (TLR2 expression by Ly6C + monocytes) or they induce internalization of the receptor that affects its turnover on the cell surface. We also observed that all EPS preparations sustained a low percentage of TNF-α positive BM monocytes even at concentrations of 100 ng/mL. In tissue-resident splenic macrophages with phenotype F4/80, however, only LY-EPS was able to increase TNF-α intracellular level. We think that other preparations might induce tonic signals that might fail to elevate TNF-α production. The significant influence of IFN-γ in F4/80 macrophages allows speculation that LY-EPS might affect IFN-γ signaling, probably via engagement with innate receptors and pathways leading to activation of IFN-γ production.

Summarizing the information on immune activity and structure of the studied biopolymers we can conclude that the LY-EPS with predominant β-bonds in the mannan-type molecule has a stronger effect on the stimulation of IFN-γ in specific immune cells relative to the more heterogeneous EPS containing in addition β-bonds and α-bonds in the molecules. The reported *in vitro* studies with peritoneal cells in mice have shown that some mannans and mannan-protein complexes stimulate the release of interferon *in vivo* and *in vitro* (Lackovic 1970). Mannans are thought to stimulate the release of IFN by a mechanism similar to that of endotoxins but in contrast, their toxicity was minimal.

For the first time, we reported an in-depth study that provided valuable insight into the composition of EPSs synthesized by Antarctic yeasts *Leucosporidium yakuticum* AL_{101} and *Cystobasidium ongulense* AL_{102}. The strains had a good capacity for the transformation of a carbon source into biomass and extracellular polysaccharide. LY was a better EPS producer and it synthesized 4.5 g/L. The chemical

nature of EPSs formed by both producers was revealed. Chemical, chromatographic and spectral studies showed that yeast strains produced high molecular weight and low molecular weight biopolymers, respectively. The high molecular weight polysaccharide synthesized by LY had a predominant mannose content, while CO-EPS contained glucose and galactose, in addition to mannose. 2D NMR study of LY-EPS revealed that mannose units were partly acetylated and at least bound by *β*-1,4 glycosidic linkages. An activation of IFN-γ in splenic F4/80 macrophages and NK cells by EPS was established and was related to their structure and monosaccharide composition enriched with mannose.

Declarations

Acknowledgment

We thank the staff of the Bulgarian Antarctic Expedition for their logistic support. The study was supported by Project 70.25-173/ 22.11.2019 of Sofia University “St. Kliment Ohridski” and the National Centre for Polar Studies in the frames of the National Program for Polar Studies 2017-2021, funded by the Bulgarian Ministry of Education and Science.

Author Contributions

Conceptualization, S.R., M.O.,Y. G., P.D.; methodology, R.S., M.O., Y.G., and P.D.; formal analysis, M.O., Y.G., M.K. and P.D.; investigation, S.R., M.O., Y.G., M.K., P.D., and A.P.; resources, S.R., M.O., M.K. and P.D.; data curation, S.R., M.O., Y.G., M.K., and P.D.; writing—original draft preparation, M.O., Y.G., S.R.; writing—review and editing, M.O., S.R., Y.G., P.D., and M.K.; visualization, S.R., M.O., and Y.G.; supervision, S.R., and M.O.; project administration, S.R.; funding acquisition, S.R.. All authors have read and agreed to the published version of the manuscript.

Conflicts of Interest:

The authors declare no conflict of interest.

References

1. Aimanianda V, Clavaud C, Simenel C, Fontaine T, Delepierre M, Latge J-P (2009) Cell Wall-(1,6)-Glucan of *Saccharomyces cerevisiae*. Structural characterization and *in situ* synthesis. J Biol Chem 284:20:13401–13412. https://doi.org/10.1074/jbc.M807667200
2. Ali P, Shah A, Hasan F, Hertkorn N, Gonsior M, Sajjad W, Chen F (2020) A glacier bacterium produces high yield of cryoprotective exopolysaccharide. Front Microbiol 10:3096. https://. doi
3. Breierová E, Hromádková Z, Stratilová E, Sasinková V, Ebringerová A (2005) Effect of salt stress on the production and properties of extracellular polysaccharides produced by *Cryptococcus laurentii*. Z Naturforsch C 60(5–6):444–450
4. Buzzini P, Margesin R (2014) Cold-Adapted Yeasts: A lesson from the cold and a challenge for the XXI Century. In: Buzzini P, Margesin R (eds) Cold-adapted Yeasts: Biodiversity, Adaptation Strategies

and Biotechnological Significance, Springer: Berlin/Heidelberg, Germany, pp 3–22

5. Chatterjee S, Mukhopadhyay SK, Gauri SS, Dey S (2018) Sphingobactan, a new α-mannan exopolysaccharide from Arctic *Sphingobacterium* sp. IITKGP-BTPF3 capable of biological response modification. Int Immunopharmacol 60:84–95. https://doi.org/10.1016/j.intimp.2018.04.039
6. Chen G, Long Yu, Zhang Y, Chang Y, Liu Y, Shen J, Xue C (2021) Utilizing heterologously overexpressed endo-1,3-fucanase to investigate the structure of sulfated fucan from sea cucumber (*Holothuria hilla*). Carbohydr Polym 272:118480. https://doi.org/10.1016/j.carbpol.2021.118480
7. Corsaro MM, Lanzetta R, Parrilli E, Parrilli M, Tutino ML, Ummarino S (2004) Influence of growth temperature on lipid and phosphate contents of surface polysaccharides from the Antarctic bacterium *Pseudoalteromonas haloplanktis* TAC 125. J Bacteriol 186:29–34. https://doi.org/10.1128/JB.186.1.29-34.2004
8. Debnath A, Das B, Devi M, Ram R (2021) Fungal exopolysaccharides: types, production and application. In: Vaishnav A, Choudhary D (eds) Microbial polymers, applications and ecological perspectives, Springer, pp 45–68
9. Donot F, Fontana A, Baccou J, Schorr-Galindo S (2012) Microbial exopolysaccharides: main examples of synthesis, excretion, genetics and extraction. Carbohyd Polym 87:951–962. https://doi.org/10.1016/j.carbpol.2011.08.083
10. DuBois M, Gilles KA, Hamilton JK, Rebers PA, Smith F (1956) Colorimetric method for determination of sugars and related substances. Anal Chem 28:350–356. https://doi.org/10.1021/ac60111a017
11. Ellefsen CF, Wold CW, Wilkins AL, Rise F, Samuelsen ABC (2021) Water-soluble polysaccharides from *Pleurotus eryngii* fruiting bodies, their activity and affinity for Toll-like receptor 2 and dectin-1. Carbohydr Polym 264:117991. https://doi.org/10.1016/j.carbpol.2021.117991
12. Freitas F, Alves V, Reis M (2011) Advances in bacterial exopolysaccharides: from production to biotechnological applications. Trends in Biotechnol 29:388–398
13. Galinari E, Sabry DA, Sassaki GL, Macedo GR, Passos FML, Mantovani HC, Rocha HAO (2017) Chemical structure, antiproliferative and antioxidant activities of a cell wall α-d-mannan from yeast *Kluyveromyces marxianus*. Carbohydr Polym 157:1298–1305. https://doi.org/10.1016/j.carbpol.2016.11.015
14. Ghada SI, Manal GH, Mohsen MS, Eman AG (2012) Production and biological evaluation of exopolysaccharide from isolated *Rhodotorula glutinins*. Aust J Basic Appl Sci 6:401–408
15. Gómez-Miranda B, Prieto A, Leal JA, Ahrazem O, Jiménez-Barbero J, Bernabé M (2004) Differences among the cell wall galactomannans from *Aspergillus wentii* and *Chaetosartorya chrysella* and that of *Aspergillus fumigates*. Glycoconj J 20:4:239–246. https://doi.org/10.1023/B:GLYC.0000025818.83019.e4
16. Gorin PAJ (1973) Rationalization of Carbon-13 magnetic resonance spectra of yeast mannans and structurally related oligosaccharides. Can J Chem 51:2375–2383
17. Gorin PAJ, Spencer JFT, Bhattachar SS (1968) Structures of yeast mannans containing both a- and β-linked D-mannopyranose units. Can J Chem 47:1499–1505

18. Hamidi M, Gholipour AR, Delattre C, Sesdighi F, Seveiri RM, Pasdaran A, Kheirandish S, Pierre G, Kozani PS, Kozani PS, Karimitabar F (2020) Production, characterization and biological activities of exopolysaccharides from a new cold-adapted yeast: *Rhodotorula mucilaginosa* sp. GUMS16. Int J Biol Macromol 151:268–277
19. Han JM, Xu Z, Liu ZM, Qian H, Zhang WG (2018) Co-production of microbial oil and exopolysaccharide by the oleaginous yeast *Sporidiobolus pararoseus* grown in fed-batch culture. RSC Adv 8:3348–3356. https://doi.org/10.1039/C7RA12813D
20. Hannuksela T, du Penhoat CH (2004) NMR structural determination of dissolved O-acetylated galactoglucomannan isolated from spruce thermomechanical pulp. Carbohydr Res 339:301–312. https://doi.org/10.1016/j.carres.2003.10.025
21. Hristova D, Rusinova-Videva S, Konstantinov S (2021) Biologically active substances and extracts offungal original. Pharmacong Rev 15:12–19
22. Huo J, Wu J, Sun B, Zhao M, Sun W, Sun J, Huang M (2020) Isolation, purification, structure characterization of a novel glucan from Huangshui, a byproduct of Chinese Baijiu, and its immunomodulatory activity in LPS-stimulated THP-1 cells. Int J Biol Macromol 161:406–416. https://doi.org/10.1016/j.ijbiomac.2020.06.028
23. Kanevskiy LM, Telford WG, Sapozhnikov AM, Kovalenko EI (2013) Lipopolysaccharide induces IFN-γ production in human NK cells. Front Immunol 4:11. https://doi.org/10.3389/fimmu.2013.00011
24. Karkhanis YD, Zeltner JY, Jackson JJ, Carlo DJ (1978) A new and improved microassay to determine 2-keto-3-deoxyoctonate in lipopolysaccharide of gram-negative bacteria. Anal Biochem 85:595–601. https://doi.org/10.1016/0003-2697(78)90260-9
25. Kato K, Nitta M, Mizuno T (1973) Infrared spectroscopy of some mannans. Agric Biol Chem 37:433–435. https://doi.org/10.1080/00021369.1973.10860687
26. Kobayashi H, Kawakami S, Ogawa Y, Shibata N, Suzuki S (2013) Structural investigation of cell wall mannan antigen obtained from pathogenic yeast *Candida zeylanoides*. Open J Med Microbiol 3:139–143. http://dx.doi.org/10.4236/ojmm.2013.32021
27. Komura DL, Carbonero ER, Gracher AHP, Baggio CH, Freitas CS, Marcon R, Santos ARS, Gorin PAJ, Iacomini M (2010) Structure of *Agaricus* spp. fucogalactans and their anti-inflammatory and antinociceptive properties. Bioresour Technol 101:15:6192–6199. https://doi.org/10.1016/j.biortech.2010.01.142
28. Lackovic V, Borecky L, Sikl D et al (1970) Stimulation of interferon production by mannans. Proc Soc Exp Biol Med 134:874–879. doi: 10.3181/00379727-134-34902
29. Leung M, Liu C, Koon J, Fung K (2006) Polysaccharide biological response modifiers. Immun Lett 105:101–114
30. Li A, Yuan F, Groenewald M, Bensch K, Yurkov A, Li K, Han P, Guo L, Aime M, Sampaio J, Jindamorakot S, Turchetti B, Inacio J, Fungsin B, Wang Q, Bai F (2020) Diversity and phylogeny of basidiomycetous yeasts from plant leaves and soil: proposal of two new orders, three new families,

eight new genera and one hundered and seven new species. Stud Micol 96:17–140. https://doi.org/10.1016/j.simyco.2020.01.002

31. Li A, Yuan F, Groenewald M, Bensch K, Yurkov A, Li K, Han P, Guo L, Aime M, Sampaio J, Jindamorakot S, Turchetti B, Inacio J, Fungsin B, Wang Q, Bai F (2020) Diversity and phylogeny of basidiomycetous yeasts from plant leaves and soil: proposal of two new orders, three new families, eight new genera and one hundered and seven new species. Stud Micology 96:17–140
32. Li Q-Z, Wu D, Zhou S, Liu Y-F, Li Z-P, Feng J, Yang Y (2016) Structure elucidation of a bioactive polysaccharide from fruiting bodies of *Hericium erinaceus* in different maturation stages. Carbohydr Polym 144:196–204. https://doi.org/10.1016/j.carbpol.2016.02.051
33. Liu X, Renard CMGC, Bureau S, Le Bourvellec C (2021) Revisiting the contribution of ATR-FTIR spectroscopy to characterize plant cell wall polysaccharides. Carbohydr Polym 262:117935. https://doi.org/10.1016/j.carbpol.2021.117935
34. Ma W et al (2018) Characterization, antioxidativity, and anticarcinoma activity of exopolysaccharide extract from *Rhodotorula mucilaginosa* CICC 33013. Carbohydr Polym 181:768–777. DOI: 10.1016/j.carbpol.2017.11.080
35. Makarova EN, Patova OA, Shakhmatov EG, Kuznetsov SP, Ovodov YS (2013) Structural studies of the pectic polysaccharide from Siberian fir (*Abies sibirica* Ledeb.). Carbohydr Polym 92:1817–1826. https://doi.org/10.1016/j.carbpol.2012.11.038
36. Makarova EN, Shakhmatov EG, Belyy VA (2018) Structural studies of water-extractable pectic polysaccharides and arabinogalactan proteins from *Picea abies* greenery. Carbohydr Polym 195:207–217. https://doi.org/10.1016/j.carbpol.2018.04.074
37. Martorell M, Ruberto L, Figueroa L, Cormack W (2019) Antarctic yeasts as a source of enzymes for biotechnological applications. In: Rosa L (ed) Fungi of Antarctica. Springer Nature Switzerland AG, pp 285–304
38. Matsuo K, Isogai E, Araki Y (2000) Occurrence of [→3)-β-D-Manp-(1→4)-β-D-Manp-(1→]$_n$ units in the antigenic polysaccharides from *Leptospira biflexa* serovar patoc strain Patoc I. Carbohydr Res 328:517–524. https://doi.org/10.1016/S0008-6215(00)00143-9
39. McComb EA, McCready RM (1957) Determination of acetyl in pectin and in acetylated carbohydrate polymers. Anal Chem 29:819–821. https://doi.org/10.1021/ac60125a025
40. Murphy EA, Davis JM, Brown AS, Carmichael MD, Ghaffar A, Mayer EP (2007) Oat beta-glucan effects on neutrophil respiratory burst activity following exercise. Med Sci Sport Exer 39:639644
41. Nandi AK, Samanta S, Sen IK, Devi KSP, Maiti TK, Acharya K, Islam SS (2013) Structural elucidation of an immunoenhancing heteroglycan isolated from *Russula albonigra*. (Krombh) Fr Carbohydr Polym 94:2:918–926. https://doi.org/10.1016/j.carbpol.2013.02.019
42. Naumenko OI, Zheng H, Wang J, Senchenkova SN, Wang H, Shashkov AS, Chizhov AO, Li Q, Knirel YA, Xiong Y (2018) Structure elucidation of the *O*-specific polysaccharide by NMR spectroscopy and selective cleavage and genetic characterization of the *O*-antigen of *Escherichia albertii* O5. Carbohydr Res 457:25–31. https://doi.org/10.1016/j.carres.2017.12.010

43. NFSS (2010) Determination of Protein in Foods. National Food Safety Standard of the People's Republic of China. China National Center for Food Safety Risk Assessment: Beijing, China, 2010. GB 5009.5–2010
44. Ognyanov M, Georgiev Y, Petkova N, Ivanov I, Vasileva I, Kratchanova M (2018) Isolation and characterization of pectic polysaccharide fraction from *in vitro* suspension culture of *Fumaria officinalis* L. Int J Polym Sci 2018:5705036. https://doi.org/10.1155/2018/5705036
45. Pavlova K, Koleva L, Kratchanova M, Panchev I (2004) Production and characterization of an exopolysaccharide by yeast. World J Microbiol Biotechnol 20:435–439. https://doi.org/10.1023/B:WIBI.0000033068.45655.2a
46. Pavlova K, Panchev I, Kratchanova M, Gocheva M (2009) Production of an exopolysaccharide by Antarctic yeast. Folia Microbiol 54:343–348
47. Pavlova K, Rusinova-Videva S, Kuncheva M, Kratchanova M, Gocheva M, Dimitrova S (2011) Synthesis and characterization of an exopolysaccharide from Antarctic yeast strain *Cryptococcus laurentii* AL_{100}. App Biochem Biothechnol 163:1038–1052. DOI: 10.1007/s12010-010-9107-9
48. Pavlova K (2014) Production of polymers and other compounds of industrial importance by cold-adapted yeasts. In: Buzzini P, Margesin R (eds) Cold-adapted yeasts. Springer, pp 397–415
49. Poli A, Anzelmo G, Tommonaro G, Pavlova K, Casaburi A, Nicolaus B (2010) Production and chemical characterization of an exopolysaccharide synthesized by psychrophilic yeast strain *Sporobolomyces salmonicolor* AL_1 isolated from Livingston Island, Antarctica. Folia Microbiol 55:576–581. https://doi.org/10.1007/s12223-010-0092-8
50. Previato JO, Vinogradov E, Silva MAE, Oliveira PAV, Fonseca LM, Maes E, Mendonça-Previato L (2019) Characterization of the 6-*O*-acetylated lipoglucuronomannogalactan a novel *Cryptococcus neoformans* cell wall polysaccharide. Carbohydr Res 475:1–10. https://doi.org/10.1016/j.carres.2019.01.012
51. Ragavan ML, Das N (2019) Optimization of exopolysaccharide production by probiotic yeast *Lipomyces starkeyi* VIT-MN03 using response surface methodology and its applications. Annal Microbiol 69:515–530. https://doi.org/10.1007/s1321 3-019-1440-9
52. Reyes-Becerril M, Angulo M, Sanchez V, Machuca C, Mendez-Martinez Y, Angulo C (2021) β–glucan bioactivities from *Cystobasidium benthicum* in *Totoaba macdonaldi* thymus cells. Fish Shellfish Immun 119:542–553
53. Rusinova-Videva S, Kambourova M, Alipieva K, Nachkova S, Simova S (2019) Metabolic profiling of Antarctic yeasts by proton Nuclear Magnetic Resonance-based spectroscopy. Biotechnol Biotechnol Eq 1:1–8
54. Rusinova-Videva S, Nachkova S, Adamov A, Dimitrova-Dyulgerova I (2020) Antarctic yeast *Cryptococcus laurentii* (AL_{65}): biomass and exopolysaccharide production and biosorption of metals. J ChemTechnol Biotech 95:1372–1379. https://doi.org/10.1002/jctb.6321
55. Rusinova-Videva S, Ognyanov M, Georgiev Y, Kambourova M, Adamov A, Krasteva V (2022) Production and chemical characterization of exopolysaccharides by Antarctic yeast *Vishniacozyma*

victoriae and *Tremellomycetes* sp. Appl Sci 12:1805. https://doi.org/10.3390/app12041805

56. Georgieva K (2011) *Effect of different carbon sources on biosynthesis of exopolysaccharide from Antarctic strain Cryptococcus laurentii AL$_{62}$*. Biotech Biotechnol Eq 25:80–84Pavlova K*)*
57. Saeed A, Paściak M, Górska S, Ceremuga I, Gamian E, Ziółkowski P, Drab M, Gamian A (2018) Structural elucidation of *Tsukamurella pulmonis* neutral polysaccharide and its visualization in infected mouse tissues by specific monoclonal antibodies. Sci Rep 8:11564. https://doi.org/10.1038/s41598-018-29864-y
58. Samuelsen ABC, Rise F, Wilkins AL, Teveleva L, Nyman AAT, Aachmann FL (2019) The edible mushroom *Albatrellus ovinus* contains a α-L-fuco-α-D-galactan, α-D-glucan, a branched (1→6)-β-D-glucan and a branched (1→3)-β-D-glucan. Carbohydr Res 471:28–38. https://doi.org/10.1016/j.carres.2018.10.012
59. Sanchez V, Rosales-Mendosa S, Monreal-Escalante E, Murillo-Alvarez J, Angulo C (2021) Conjugation of β-glucans on heat-stable enterotoxins (ST) to enchance the immunogenic response in mouse leucocytes. Mat Sci & Eng C 118:111464
60. Seveiri MR, Hamidi M, Delattre C, Rahmani B, Darzi S, Pierre G, Sedighian H (2019) Characterization of the exopolysaccharides from *Rhodotorula minuta* IBRC-M 30135 and evaluation of their emulsifying, antioxidant and antiproliferative activities. Med Sci 23:381–389
61. Shakhmatov EG, Makarova EN (2022) Structure of KOH-extractable polysaccharides of tree greenery of from Siberian fir *Abies sibirica* Ledeb. Carbohydr Polym 276:118794. https://doi.org/10.1016/j.carbpol.2021.118794
62. Shibata N, Ikuta K, Imai T, Satoh Y, Satoh R, Suzuki A, Kojima C, Kobayashi H, Hisamichi K, Suzuki S (1995) Existence of branched side chains in the cell wall mannan of pathogenic yeast, *Candida albicans*. Structure-antigenicity relationship between the cell wall mannans of *Candida albicans* and *Candida parapsilosis*. J Biol Chem 270:3:1113–1122. https://doi.org/10.1074/jbc.270.3.1113
63. Synytsya A, Čŏpíková J, Matějka P, Machovič V (2003) Fourier transform Raman and infrared spectroscopy of pectins. Carbohydr Polym 54:97–106. https://doi.org/10.1016/S0144-8617(03)00158-9
64. Tang N, Wang X, Yang R, Liu Z, Liu Y, Tian J, Xiao L, Li W (2022) Extraction, isolation, structural characterization and prebiotic activity of cell wall polysaccharide from *Kluyveromyces marxianus*. Carbohydr Polym 289:119457. https://doi.org/10.1016/j.carbpol.2022.119457
65. Tsuji M, Tsujimoto M, Imura S (2017) *Cystobasidium tubakii* and *Cystobasidium ongulense*, new basidiomycetous yeast species isolated from East Ongul Island, Est Antarctica. Micosci 58:103–110. 10.1016/j.myc.2016.11.002
66. Turkiewicz M, Pazgier M, Donachie SP, Kalinowska H (2005) Invertase and a-glucosidase production by the endemic antarctic marine yeast *Leucosporidium antarcticum*. Pol Polar Res 26:125–136 ISSN 0138–0338; eISSN 2081–8262
67. Turkiewicz M, Pazgier M, Kalinowska H, Bielecki S (2003) A cold-adapted extracellular serine proteinase of the yeast *Leucosporidium antarcticum*. Extremophiles 7:435–442

68. Ustyuzhanina NE, Kulakovskaya EV, Kulakovskaya TV, Menshov VM, Dmitrenok AS, Shashkov AS, Nifantiev NE (2018) Mannan and phosphomannan from *Kuraishia capsulata* yeast. Carbohydr Polym 181:624–632. https://doi.org/10.1016/j.carbpol.2017.11.103
69. Van Bogaert INA, De Maeseneire SL, Vandamme EJ (2009) Extracellular polysaccharides produced by yeasts and yeast-like fungi. In: Satyanarayana T, Kunze G (eds) Yeast Biotechnology: Diversity and Applications. Springer Science + Business Media, B.V.:Berlin/Heidelberg, Germany, pp 651–671
70. Vishniac HS (2006) Yeast biodiversity in the Antarctic. In: Rosa CA, Peter G (eds) Biodiversity and ecophysiology of yeasts. Springer, Berlin, pp 420–440
71. Wiley SR, Schooley K, Smolak PJ et al (1995) Identification and characterization of a new member of the TNF family that induces apoptosis. Immunity 3:673–682
72. Hao Y et al (2020) Exopolysaccharide from *Cryptococcus heimaeyensis* S20 induces autophagic cell death in non-small cell lung cancer cells via ROS/p38 and ROS/ERK signaling. Cell Prolif 53. https://doi.org/10.1111/cpr.12869
73. Yamada H, Ohshima Y, Miyazaki T (1982) Characterisation of fucomannopeptide and mannoprotein from *Absidia cylindrospora*. Carbohydr Res 110:113–126. https://doi.org/10.1016/0008-6215(82)8
74. Yang L, Zhang L (2009) Chemical structural and chain conformational characterization of some bioactive polysaccharides isolated from natural sources. Carbohyd Polym 76:349361
75. Zhang M, Qin H, An R, Zhang W, Liu J, Yu Q, Liu W, Huang X(2022) Isolation, purification, structural characterization and antitumor activities of a polysaccharide from *Lilium davidii* var. *unicolor* Cotton J Mol Struct 1261:132941. https://doi.org/10.1016/j.molstruc.2022.132941
76. Zhang S, Qiao Z, Zhao Z, Guo J, Lu K, Mayo KH, Zhou Y (2021) Comparative study on the structures of intra- and extra-cellular polysaccharides from *Penicillium oxalicum* and their inhibitory effects on galectins. Int J Biol Macromol 181:793–800. https://doi.org/10.1016/j.ijbiomac.2021.04.042
77. Zhang Z, Zhou Z, Li Y, Zhou L, Ding Q, Xu L (2016) Isolated exopolysaccharides from *Lactobacillus rhamnosus* GG alleviated adipogenesis mediated by TLR2 in mice. Sci Rep 6:36083. https://doi.org/10.1038/srep36083)
78. Zhou X, Hong T, Yu Q, Nie S, Gong D, Xiong T, Xie M (2017) Exopolysaccharides from *Lactobacillus plantarum* NCU116 induce c-Jun dependent Fas/Fasl-mediated apoptosis via TLR2 in mouse intestinal epithelial cancer cells. Sci Rep 27(1):14247. doi: 10.1038/s41598-017-14178-2. PMID: 29079852; PMCID: PMC5660251
79. Zhou Y, Cui Y, Qu X (2019) Exopolysaccharides of lactic acid bacteria: structure, bioactivity and associations: a review. Carbohydr Polym 207:317–332. doi: 10.1016/j.carbpol.2018.11.093

Tables

Table 1 Yield, monosaccharide composition, and protein content of EPSs

	CO-EPS	LY-EPS
Yield, g EPS/100 g[1] (g EPS/L)[2]	3.4 (1.3)	11.7 (4.5)
Total carbohydrates[3], w/w%	62	80
Mannose	30 (42)[4]	78 (90)
Glucose	20 (28)	0 (0)
Xylose	Trace	4 (5)
Galactose	16 (22)	0 (0)
Fucose	Trace	Trace
Uronic acids	5.7 (8)	4.7 (5)
Rare sugars test	-	-
Acetyl content, w/w%	1.4	0.4
Protein, w/w% (N×5.78)	30	18

[1] per dry weight biomass; [2] to a liter of cultural liquid; [3] mannose equivalent; [4] Values in brackets represent the monosaccharide composition in mol%.

Table 2 ^{13}C and ^{1}H chemical shifts (δ, ppm) of LY-EPS, referenced to DSS[b]

Residue	C-1	C-2	C-3	C-4	C-5	C-6
	H-1	H-2	H-3	H-4	H-5,5'	H-6
→4)-*β*-Man*p*-(1→	97.6	70.9	72.2	77.4	75.6	61.2
	4.85	4.12	3.84	3.85	3.51	3.88; 3.75
→4,3)-*β*-Man*p*-(1→	100.7	68.3	79.9	77.4	76.7	61.2
	4.72	4.23	3.93	3.85	3.47	3.73
β-Man*p*-(1→	100.7	70.9	72.2	65.8	76.7	61.2
	4.72	4.06	3.83	3.71	3.47	3.73
α-Fuc*p*-(1→	98.2	n.d.*	n.d.	71.1	70.9	15.9
	4.97	3.71	3.90	4.06	4.23	1.21
β-Xyl*p*-(1→	101.2	73.8	n.d.	68.5	64.5	-
	4.59	3.34	3.47	3.63	3.95	

*not determined

b - Sodium 4,4-dimethyl-4-silapentane-sulfonate was used as an internal standard. Add 2.1 (2.07) ppm to each value of the carbon atoms to obtain the chemical shifts with respect to the internal standard

Table 3 ^{13}C and ^{1}H chemical shifts (δ, ppm) of CO-EPS, referenced to DSS[b]

Residue	C-1	C-2	C-3	C-4	C-5	C-6
	H-1	H-2	H-3	H-4	H-5,5'	H-6
→4)-*β*-Man*p*-(1→	97.6	70.9	72.2	77.4	75.6	61.6
	4.85	4.12	3.83	3.86	3.51	3.76; 3.87
→4,3)-*β*-Man*p*-(1→	100.6	68.3	79.9	77.4	76.7	61.6
	4.73	4.24	3.93	3.86	3.46	3.75
→4)-*β*-Man*p*-3-*O*Ac-(1→	100.6	69.8	74.9	73.8	76.2	61.6
	4.73	4.14	5.03	4.04	3.53	3.76; 3.88
→2)-*α*-Man*p*-(1→	101.1	79.0	70.9	65.7	73.8	61.6
	5.25	4.07	3.92	3.74	3.75	3.76; 3.87
→2)-*α*-Man*p*-(1→	102.7	83.7	70.9	67.7	73.8	61.6
	5.07	4.07	3.92	3.69	3.75	3.76; 3.87
→2,6)-*α*-Man*p*-(1→	102.7	83.7	70.9	67.7	73.8	66.5
	5.11	4.02	3.92	3.69	3.75	4.02; 3.77
α-Man*p*-(1→2)	102.7	70.9	72.2	67.7	73.8	61.6
	5.05	4.12	3.83	3.69	3.75	3.90
α-Man*p*-(1→	102.7	70.7	72.2	70.3	72.1	61.2
	5.07	4.07	3.85	3.52	3.83	3.69
→2,3)-*α*-Man*p*-(1→	102.7	78.0	81.9	n.d.*	n.d.	61.6
	5.07	4.07	4.12	3.56	3.68	3.85
→6)-*α*-Gal*p*-(1→	98.6	68.9	70.3	70.2	69.5	67.2
	4.96	3.84	3.88	4.02	4.20	3.69; 3.90
→6)-3-*O*-Me-α-Gal*p*-(1→	98.4	68.9	80.4	66.6	69.5	67.2
	4.97	3.88	3.53	4.30	4.20	3.69; 3.90
→2,6)-*α*-Gal*p*-(1→	98.6	80.4	70.3	70.2	69.5	67.2
	5.11	3.96	4.02	4.07	4.20	3.70; 3.91
α-Fuc*p*-(1→	100.0	n.d.	n.d.	71.3	69.8	18.3
	4.91	3.80	3.88	4.02	4.27	1.27
→1)-*β*-Gal*p*-(4→	105.2	71.9	73.4	80.4	76.3	61.5
	4.65	3.58	3.72	4.02	3.76	3.69

β-Glc*p*-(1→	103.3	73.4	75.5	70.4	76.6	63.5
	4.73	3.36	3.53	3.42	3.48	3.73
→3)-Glc*p*-(1→	103.3	76.3	85.1	70.2	76.3	63.5
	4.78	3.56	3.72	3.52	3.69	3.86
→6)-*β*-Glc*p*-(1→	103.3	73.4	75.5	70.3	76.3	68.9
	4.53	3.34	3.53	3.47	3.69	4.20; 3.86
→3,6)-*β*-Glc*p*-(1→	103.1	76.3	85.1	71.8	76.3	68.9
	4.57	3.53	3.77	3.58	3.69	4.20; 3.86
→4)-*α*-Glc*p*-(1→	99.5	72.1	73.4	78.0	71.9	61.2
	5.36	3.58	3.88	3.64	3.76	3.84
α-Ara*f*-(1→	109.7	81.9	78.9	82.9	61.5	-
	5.21	4.20	4.02	4.12	3.76; 3.83	
α-Ara*f*-(1→	107.7	81.9	78.9	83.7	61.5	-
	5.27	4.12	3.96	4.07	3.85; 3.74	
→5)-*α*-Ara*f*-(1→	108.5	81.9	78.9	82.8	67.2	-
	5.05	4.12	4.02	4.20	3.90	

*not determined

b - Sodium 4,4-dimethyl-4-silapentane-sulfonate was used as an internal standard. Add 2.1 (2.06) ppm to each value of the carbon atoms to obtain the chemical shifts with respect to the internal standard

Figures

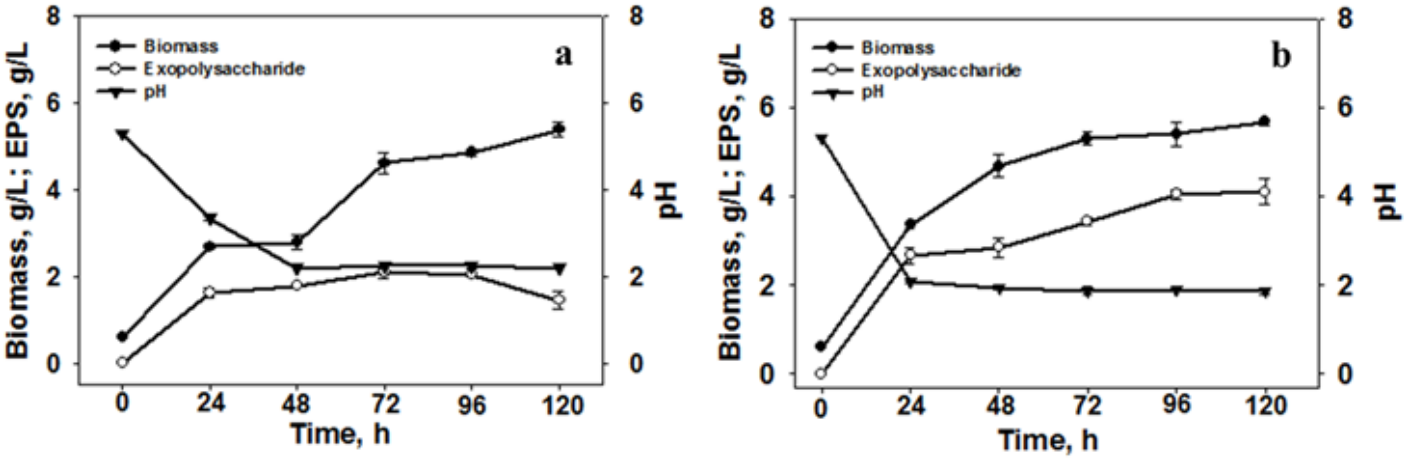

Figure 1

Time course of cell growth, EPS accumulation, and pH during the submerged cultivation of A) *C. ongulense* AL_{101} and B) *L. yakuticum* AL_{102}

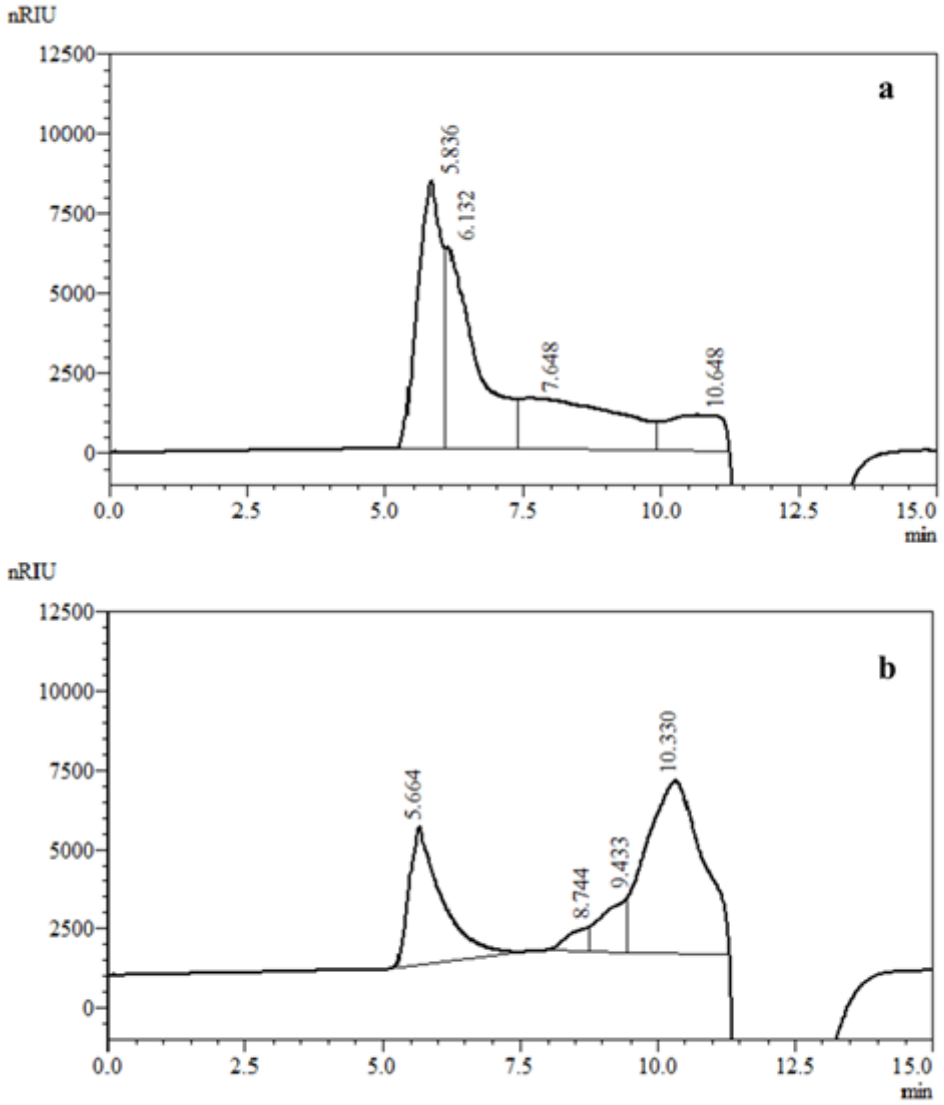

Figure 2

HPSEC elution pattern of EPS produced by: (**a**) *Leucosporidium yakuticum* AL_{102} (**b**) *Cystobasidium ongulense* AL_{101}. Pullulan standards (0.59×10^4 to 78.8×10^4 g/mol Mw range) were used to estimate the molecular weights

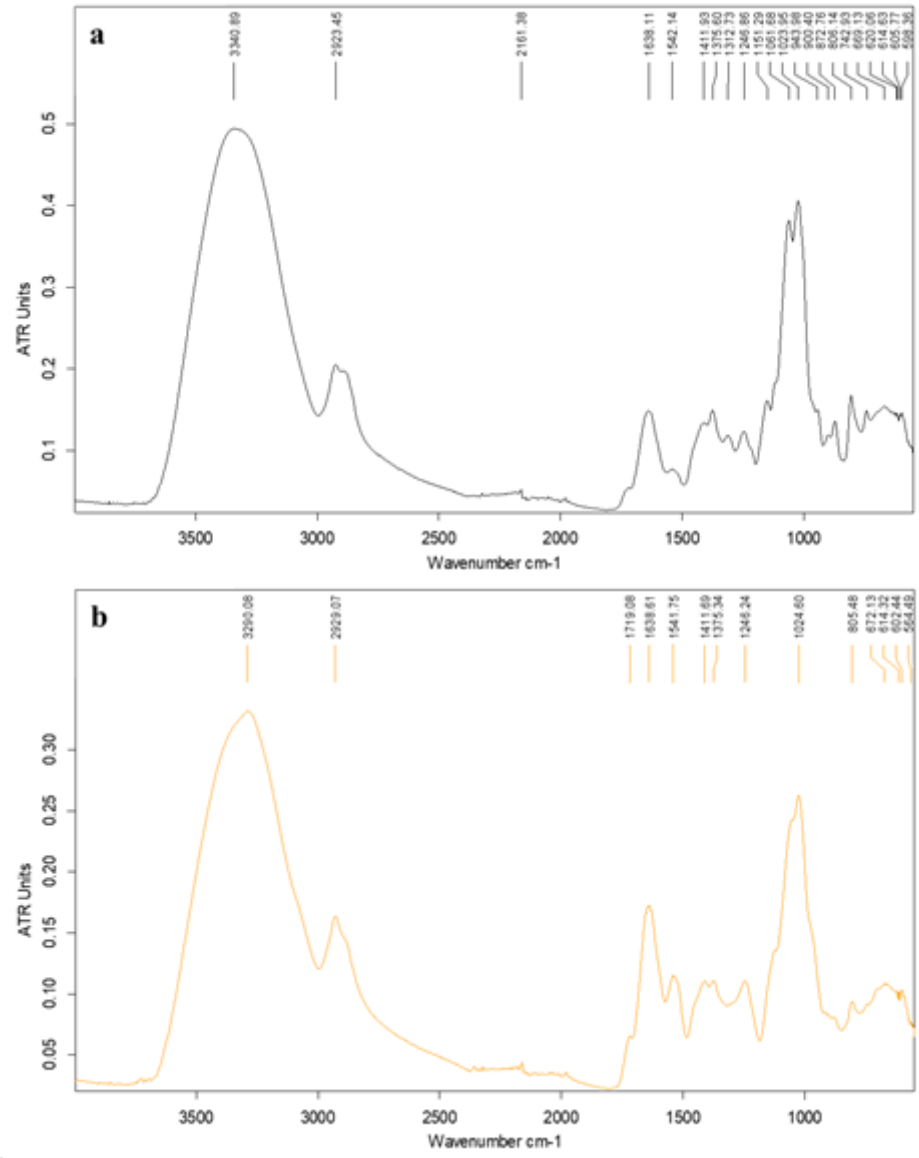

Figure 3

FT-IR spectra of EPS produced by: a) *Cystobasidium ongulense* AL_{101}; b) *Leucosporidium yakuticum* AL_{102}

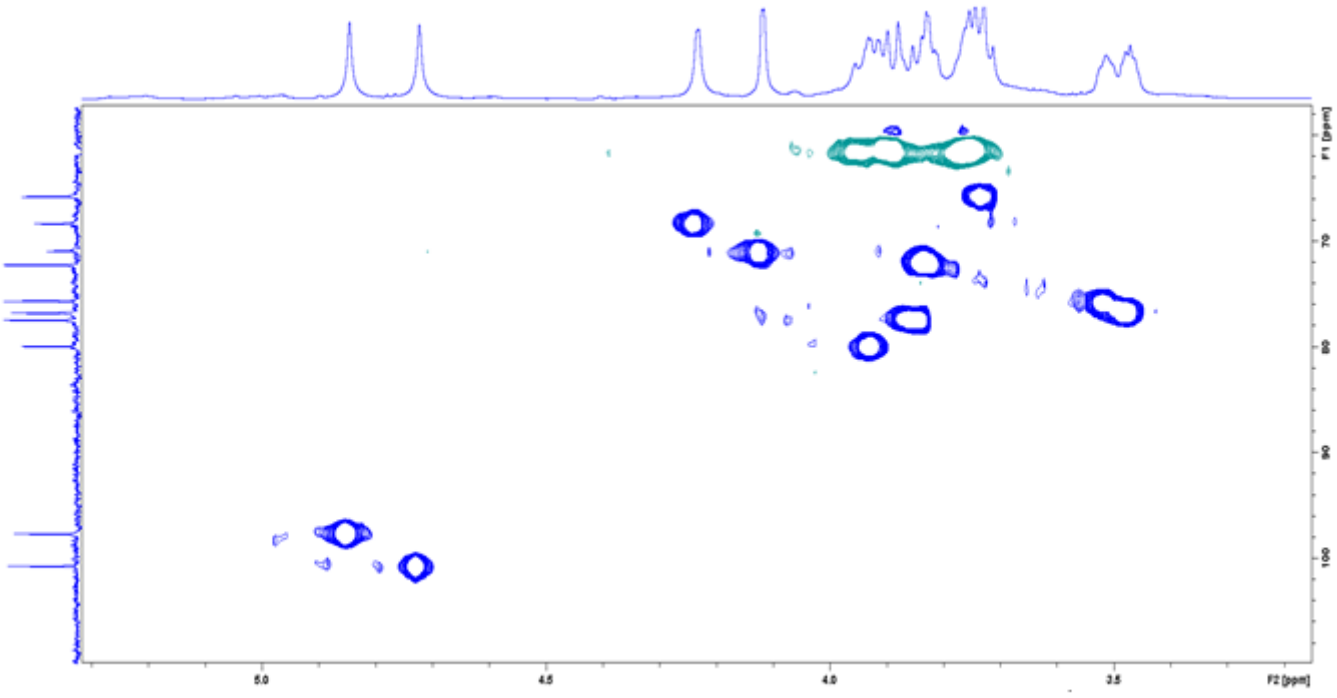

Figure 4

Fragment of $^{1}H/^{13}C$ HSQC spectrum of *L. yakuticum* -EPS. Sodium 4,4-dimethyl-4-silapentane-sulfonate was used as an internal standard

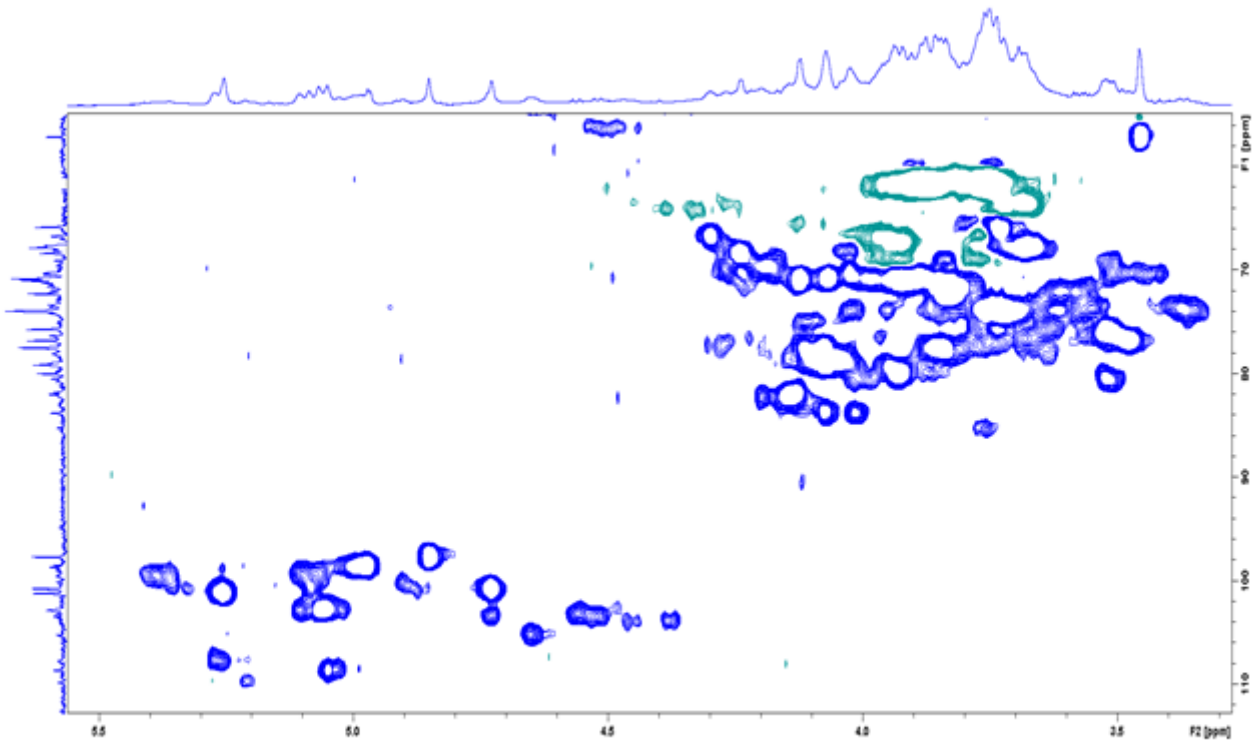

Figure 5

Fragment of $^{1}H/^{13}C$ HSQC spectrum of *C. ongulense* -EPS. Sodium 4,4-dimethyl-4-silapentane-sulfonate was used as an internal standard

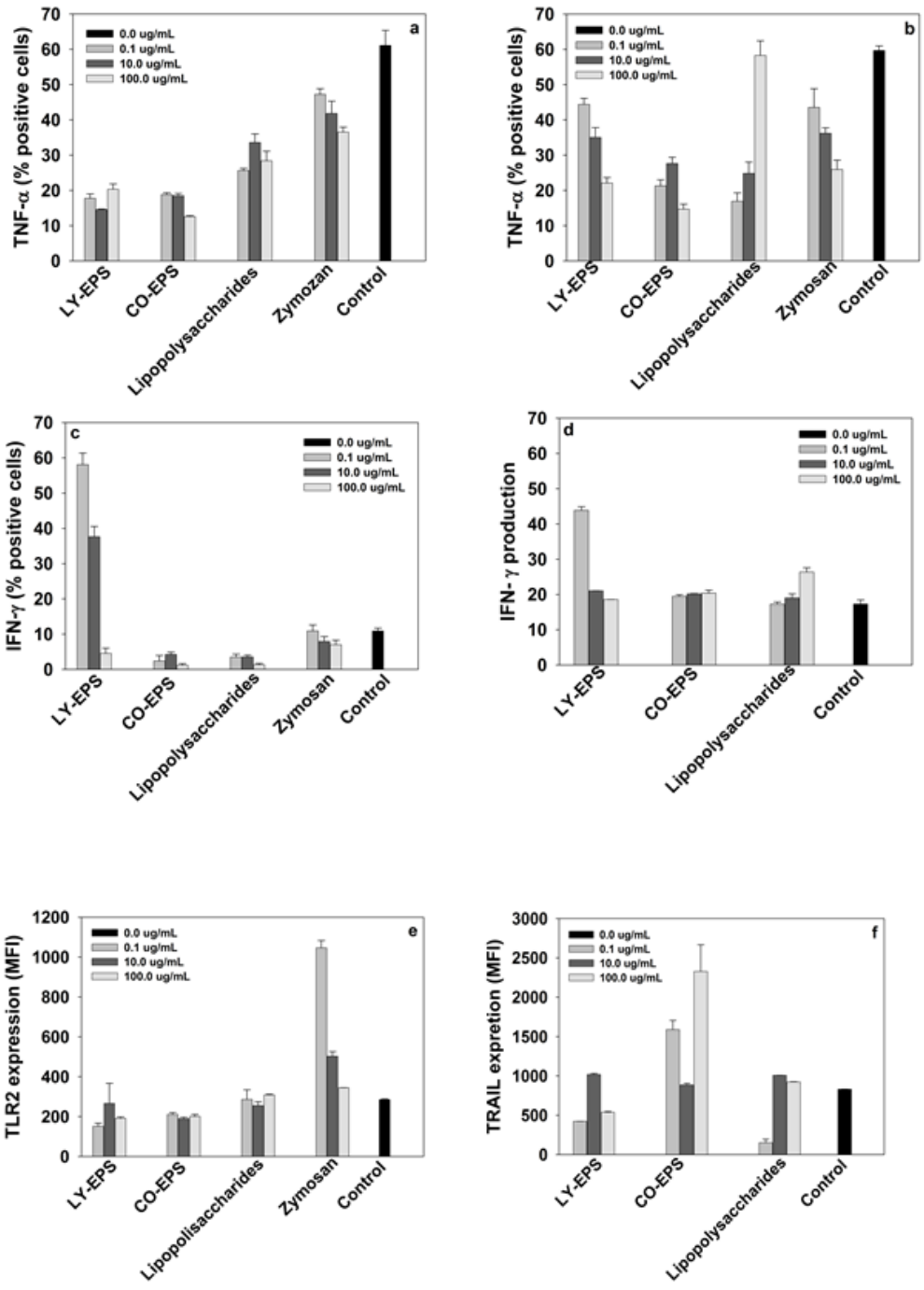

Figure 6

Effect of exopolysaccharide solutions (*L. yakuticum*-EPS and *C. ongulense* -EPS) on intracellular a) TNF-α production in Ly6C+ monocytes; b) TNF-α production in F4/80 macrophages; c) IFN-g production in F4/80 macrophages; d) IFN-g production by splenic NK cells; e) on TLR2 expression by Ly6C+ monocytes; f) on TRAIL expression by splenic NK cells

Supplementary Files

This is a list of supplementary files associated with this preprint. Click to download.

- Supplementary.docx